Becken, M., Ritter, O. (2011): Magnetotelluric Studies at the San Andreas Fault Zone: Implications for the Role of Fluids. - Surveys in Geophysics, 33, 1, 65-105

DOI: 10.1007/s10712-011-9144-0

Editorial Manager(tm) for Surveys in Geophysics
Manuscript Draft

Manuscript Number:

Title: MT studies at the San Andreas Fault Zone: Implications for the role of fluids

Article Type: Special Issue - EMIW Giza2010

Keywords: Magnetotellurics; San Andreas Fault; Fluids.

Corresponding Author: Michael Becken

Corresponding Author's Institution: Institute of Geophysics, WWU Muenster

First Author: Michael Becken

Order of Authors: Michael Becken;Oliver Ritter

Fluids residing in interconnected porosity networks have a significant weakening effect on rheology of rocks and can strongly influence deformation along fault zones. The magnetotelluric (MT) technqiue is sensitive to interconnected fluid networks, and can image these zones on crustal and upper mantle scales. MT has imaged several prominent electrically conductive anomalies at the San Andreas fault which have been attributed to the presence of saline fluids within such networks, and which have been associated with tectonic processes. These models suggest that ongoing fluid release in the upper mantle and lower crust is closely related to the mechanical state of the crust. Where fluids are drained into the brittle portion of the crust, and where these fluids are kept at high pressures, fault creep is supported. In response to fluid flux from deeper levels in combination with meteoric and crustal metamorphic fluid supply, and in response to fault creep, high-conductivity zones develop as fault zone conductors in the brittle portion of crust. In turn, the absence of crustal fluid pathays may be characteristic for mechanically locked segments. MT models suggest that those fluids are trapped at depth and kept at high pressures. It is speculated that fluids may infiltrate neighbouring rocks and induce non-volcanic tremor.

Surv. Geophys. manuscript No.
(will be inserted by the editor)

MT studies at the San Andreas Fault Zone: Implications for the role of fluids

Michael Becken and Oliver Ritter

the date of receipt and acceptance should be inserted later

Abstract Fluids residing in interconnected porosity networks have a significant weakening effect on rheology of rocks and can strongly influence deformation along fault zones. The magnetotelluric (MT) technqiue is sensitive to interconnected fluid networks, and can image these zones on crustal and upper mantle scales. MT has imaged several prominent electrically conductive anomalies at the San Andreas fault which have been attributed to the presence of saline fluids within such networks, and which have been associated with tectonic processes. These models suggest that ongoing fluid release in the upper mantle and lower crust is closely related to the mechanical state of the crust. Where fluids are drained into the brittle portion of the crust, and where these fluids are kept at high pressures,

M. Becken

GFZ German Research Centre for Geosciences, Telegrafenberg, 14473 Potsdam, Germany

E-mail: michael.becken@uni-muenster.de

Present address: WWU, Corrensstr. 24, 48149 Münster, Germany

O. Ritter

GFZ German Research Centre for Geosciences, Telegrafenberg, 14473 Potsdam, Germany

fault creep is supported. In response to fluid flux from deeper levels in combination with meteoric and crustal metamorphic fluid supply, and in response to fault creep, high-conductivity zones develop as fault zone conductors in the brittle portion of crust. In turn, the absence of crustal fluid pathays may be characteristic for mechanically locked segments. MT models suggest that those fluids are trapped at depth and kept at high pressures. It is speculated that fluids may infiltrate neighbouring rocks and induce non-volcanic tremor.

1 Introduction

California is one of the most earthquake-prone regions of the world. Most occurrences of earthquakes are attributed to the San Andreas Fault (SAF) system, which runs the entire length of California. Major earth science initiatives such as the San Andreas Fault Observatory a Depth (SAFOD), a deep borehole intersecting the SAF at 3.2 km depth (Hickman et al. 2004), and a range of geological, geochemical, and geophysical exploration and monitoring programs have tremendously increased our knowledge about physical and chemical processes within and surrounding of the fault zone, making the SAF the best studied fault zone on Earth. However, fundamental properties of the fault such as fault strength and fault geometry at deeper levels are not fully understood, and a unifying model that could explain all spatial and temporal variability of seismicity along the fault is still a vision.

Many of the seismological observations, including aseismic slip along distinct segments of the SAF (Irwin and Barnes 1975) and companion faults and the occurrence of non-volcanic tremor at lower crustal and upper mantle depth (Nadeau

and Dolenc 2005) are explained with fluid-related processes, as fluids can strongly influence the mechanical strength of rocks. Fluids at high pressures have the ability to reduce the strain threshold of rocks and facilitate brittle failure within the upper crust (Byerlee 1990; Scholz 2002). At deeper levels, below the seismogenic zone where rocks exhibit a ductile (or viscous) style of deformation, the presence of fluids can also dramatically reduce the shear strength. The effect of weakening will be more severe if fluids form an interconnected network, i.e. in pores, cracks, or veins (Bürgmann and Dresen 2008). In turn, a high degree of pore interconnectivity may indicate a region with a high degree of strain, i.e. a zone that has undergone substantial deformation during its tectonic history.

Bulk electrical conductivity of a subsurface volume depends strongly on the presence of conductive phases within such interconnected networks (Gueguen and Palciauskas 1994) and measurements of electrical conductivity are therefore one of the best means to constrain the volume of available fluids and the regions of high strain. In turn, electrical conductivity can be used to constrain rock strength in the lower crust and upper mantle.In addition to aqueous fluids and partial melts, conductive minerals such as graphite may account responsible for conductive MT anomalies (Ritter et al. 2003; Unsworth et al. 2000). MT is not able to distinguish unambiguously between conductive fluids and other conductive phases at depth, but irrespective of the particular phase being conductive, it must possess long-range interconnection to respond to MT measurements.

If fluids are responsible for high electrical conductivity of a subsurface volume, then the implication for rock strength can be two-fold. First, the presence of fluids (at high pressures) has a weakening effect itself. Unsworth (2010) summarized some empirical relationships between electrical resistivity and rock strength

in the presence of fluids and based on laboratory experiments. Second, electrical conductivity is elevated only if those fluids possess interconnection. Porosity networks may have developed in high strain regions, which may represent *per se* weak zones, and which are just illuminated if fluid-filled. Naturally, presence of fluids and existence of porosity networks are coupled phenomena, and it may be difficult to identify cause and effect or to separate their influence on rock strength.

MT studies at the SAF, and at many other active and fossil tectonic systems, imaged electrical conductivity anomalies on various crustal and upper mantle scales, which seem closely related to active or ancient tectonic processes. Many of the high-conductivity anomalies associated with active tectonic settings are plausibly interpreted with saline or hydrothermal aqueous fluids residing in interconnected porosity networks. If so, a deeper understanding of the resistivity structure can be obtained by addressing (i) the fluid sources, and the mechanisms or chemical reaction releasing these fluids (ii) mechanisms which can account for the required degree of pore interconnectivity (iii) the distribution and generation of pathways and barriers for fluid flow.

All of these aspects have fault-related implications. For instance, where the SAF exhibits aseismic creep or a combination of microseismicity and creep, the upper few kilometers of the fault are characterized by a wedge-shape zone of high conductivity associated with fluids circulating in the damage zone of the fault, and denoted as the fault zone conductor (FZC) (e.g. Ritter et al. 2005; Bedrosian et al. 2004; Unsworth et al. 2000). The FZC is characteristically devoid of seismicity, suggesting that this region is rheologically extremely weak (Unsworth et al. 2000). Along-strike variations of the FZCs magnitude have been associated with the fault activity (Hoffmann-Rothe et al. 2004; Ritter et al. 2005), as active

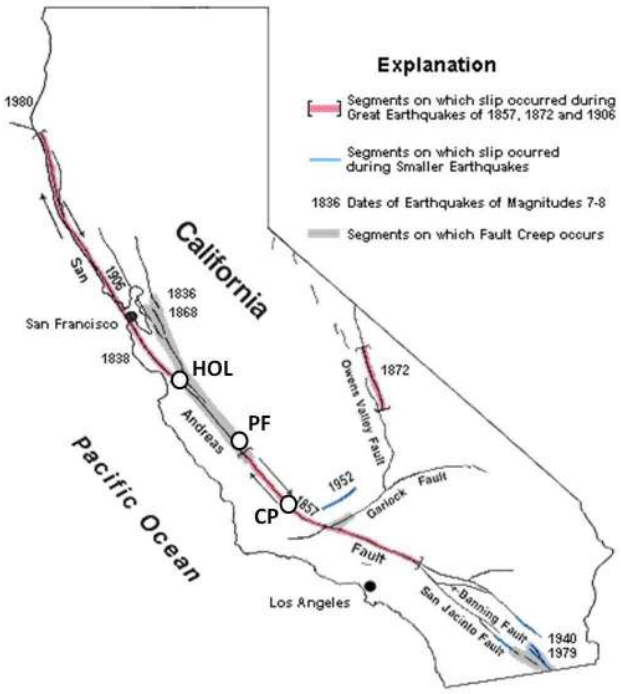

Fig. 1 Map of California showing segments of the SAF system where fault exhibits creep (gray shaded), and distribution of ruptures associated with historical earthquakes (red shaded). Locations of MT study areas near Hollister (HOL), Parkfield (PF) and Carrizo Plain (CP) are indicated. Background map provided by US Geological Survey (http://pubs.usgs.gov/gip/earthq3/where.html)

strain provides a means to develop and maintain permeability structure, and thus electrical conductivity, within the damage zone. Accordingly, these conductivity models played an important role in pin-pointing the SAFOD drilling location near Parkfield.

In this paper, we consider MT studies at the SAF near Hollister and Carrizo Plain, respectively, and from the Parkfield-Cholame segment in Central California. The existing MT studies at Carrizo Plain (Mackie et al. 1997; Unsworth et al. 1999) and Hollister (Bedrosian et al. 2004) focused on imaging upper crustal re-

sistivity structure and its relationship to the SAF and companion fault zones. By far the most MT data are available from the Parkfield-Cholame segment in central California, where a number of fine-scale (Unsworth et al. 2000; Unsworth and Bedrosian 2004; Unsworth et al. 1997, 1999) and regional scale studies (Eberhart-Philips et al. 1995; Becken et al. 2008, 2011) were carried out to investigate both the zone of seismogenesis along the SAF as well as the deeper roots of the fault system in the lower crust and upper mantle.

A recent offshore marine MT survey (Wheelock et al., 2010, reference missing) complements the regional scale land studies in central California. These data are presently analyzed and not yet available to become included in this review. Offshore or amphibic MT data can be of particular value in order to address (i) actively deforming strands of the SAF system located offshore (e.g. Hosgri fault, see Wilson et al. 2005) (ii) the role of the Montery Microplate, believed to be partially subducted beneath continental North America and believed to influence the developmemt of the transform margin as well as its present state (e.g. McCrory et al. 2009; Popov 2009) (iii) the coast effect, a term used to describe the effect of the high-conductance ocean body on the MT responses measured far inland Schmucker (e.g. 1970).

The SAF has also been a target for telluric (Madden et al. 1993; Park et al. 2007) and magnetotelluric monitoring (e.g. Kappler et al. 2010). These installations attempted to monitor long-term electric (and magnetic) field variations of internal origin due to resistivity variations assiciated with earthquakes, large scale fluid flow or other causes. To date, it was not possible to identify significant field variations which can be attributed to tectonic processes. In this paper, we don't discuss details of this issue.

The main objective of this paper is to review the MT results from the SAF in combination with other geophysical, geological and geochemical data and models in order to address fluid-related processes and their potential implications on the geodynamic setting, active tectonic processes and the mechanical state of the fault. In combination, many of these observations support a scenario which suggests that fluids derived from the mantle strongly influence the mechanics of the fault system. This scenario is largely based on studies at the Parkfield-Cholame segment, where the SAF is transitional from mechanical lock to aseismic creep, and where a remarkable consistency between fluid distribution (based on MT model interpretation), fluid chemistry, seismological patterns and geodynamical and mechanical models was found.

The paper is organized in two main parts. In the first part (section 2), we discuss the relationship between resistivity structure, fluids and possible implications for the strength of the brittle SAF. In the second part (section 3), regional-scale fluid related processes are discussed based on MT models and other studies from the Parkfield-Cholame area. These two parts are clearly dependent on each other, because a deeper regional-scale fluid source has been proposed to contribute to the fluid budget in the upper crust, at least where the fault is aseismic, and because near-surface observations indicate the existence of such a deep fluid source.

2 Fluid distribution and fault strength

Earthquakes on the San Andreas fault mostly range between depths of 2 and 15 km and provide information about the location and style of deformation of the fault in this upper-crustal 'seismogenic' zone, where rocks fail in a brittle way.

The seismogenic zone of the SAF is particularly well defined through earthquake 'curtains' along the segments of the fault which exhibit a combination of aseismic slip and frequent microseismicity.

Aseismically creeping zones anticorrelate with zones which have been ruptured by major earthquakes in historical times, and which are locked since then. The largest recorded earthquakes along the SAF occurred in 1857 in southern California and 1906 in San Francisco with magnitudes of approximately 8. The 1857 Fort Tejon earthquake nucleated near Parkfield and propagated southeastward for over a length of 360 km. The great 1906 San Francisco earthquake ruptured the northern segment of the fault, from Hollister northward, for 400 km. Since then, both segments appear to be locked (except for smaller ruptures associated with earthquakes such as the M7.1 Loma Prieta earthquake in 1989 and the M6.6 earthquake near Los Angeles in 1994). Between Parkfield and north of Hollister, the SAF exhibits a combination of aseismic creep and microseismicity; at Parkfield, characteristic M6 earthquakes, the last in 2004, have occurred, whereas constant steady movement of about 2-4 centimeters per year and only minor quakes characterize the rest of the creeping segment (Irwin 1990, cf. Figure 1).

Early explanations of the difference in seismic behavior of the SAF emphasized the role of fluids released by metamorphic reactions (Figure 4c, after Irwin and Barnes 1975). Fluids at high pressures play also a key role in more recent modelling scenarios which attempt to address the weakness of the fault where it exhibits aseismic creep (e.g. Fulton and Saffer 2009). MT has proven a valuable tool to image fluids present in the subsurface, and a number of MT studies across the SAF studies have delineated high-conductivity zones associated with the upper few kilometers of the SAF, which are thought to support mechanical models of fluid-

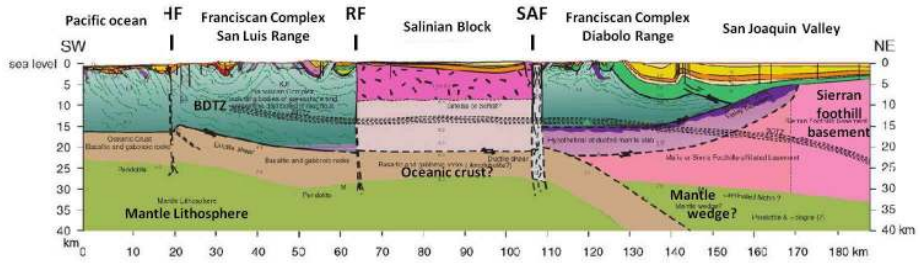

Fig. 2 Geological cross-section across the Coast Ranges and the SAF near Cholame in Central California, based on the compilation of geophysical and geological data by Page et al. (1998) and simplified by Zoback et al. (2002). A rigid block of Salinian granite intervenes between intensively deformed rocks of the Franciscan Formation, and is bounded by the SAF to the east and Rinconada fault, a subparallel strand of the SAF, to the west.

weakening. In what is to follow in this section, we discuss those MT results and their potential implications on understanding fluid-related fault characteristics. We start this section with a brief geological description.

2.1 Geological setting

In central California, total displacement of the Pacific plate relative to fixed North America is estimated to about 820 ± 50 km (Nicholson et al. 1994), and has been distributed over various fault strands (Dickinson et al. 2005) since subduction of Farallon oceanic plate ceased and the SAF system was initiated 20 Ma ago. Among these strands of the fault system, the central SAF has accomodated about 315 km displacement. As a result, the geological formations along the continental margin were substantially reorganized since the transform margin evolved, and the deformation along the SAF system has shaped the landscape of present California.

Today, the SAF system criss-crosses three major geologic formations which constitute the Californian Coast Ranges: the Franciscan complex, the Salinian Block and the Great Valley sequence. These geological units form northwest-southeast trending belts. In brief, the Franciscan rocks represent pieces of oceanic lithosphere that have been accreted to North America by subduction and collision prior to the development of the transform margin. They comprise sandstones and shale, carrying fragments of cherts and other rocks, low-grade metmorphosed volcanic rocks in greenschist facies, higher-grade blueschists, as well as disrupted pieces of the Coast Range ophiolite representing oceanic crust and mantle rocks. The major component of the Salinian Block is granitic plutonic rocks, similar in composition, chemistry and age to those of the Sierran batholith constituting the Sierra Nevada. As part of the Pacific plate, the Salinian block has been transported along the SAF in the northeast direction to its present position. Sediments of the Great valley sequence were originally deposited in the forearc basin of the Farallon subduction zone under marin condititons. All of these rocks have experienced substantial deformation and displacement during their subduction and transform motion history.

The SAF in Central California juxtaposes the Salinian block, formally part of the Pacific plate, against Franciscan formation accreted to the North American plate. The Salinian Block is intervening between the SAF and westward located strands of the transform fault system. Figure 2 presents a simplified geological cross-section across the SAF near Cholame in Central California, which is based on seismic reflection and refraction data, magnetic and gravity maps and geological mapping (Page et al. 1998). Whereas upper crustal structure is relatively well constrained by seismic data and geological evidence, deeper structure and in par-

ticular the existence of a remant slab extending to the SAF or farther east and documenting former subduction along coastal California, must be looked at more carefully.

2.2 Earthquakes and Fault creep

The apparent low frictional strength of the SAF, where it exhibits creep, is poorly understood. The lack of an observable heat flow anomaly near the fault, as expected from frictional heat generation, has been interpreted to indicate that the effective friction coefficient along the SAF is 0.2 (e.g. Sass et al. 1997) or less. Mechanical modelling of the fault behavior determined friction coefficients of less than 0.1 within the fault (Fulton and Saffer 2009; Popov 2009) in order to explain an active fault plane oriented at high angle to the maximum principal stress direction (e.g. Fulton and Saffer 2009) as has been observed within the SAFOD pilot and main holes (Hickman et al. 2004; Zoback et al. 2006) and inferred for other segments of the SAF (Townend and Zoback 2004). Explanations include high pore fluid pressures within the fault zone or the presence of weak minerals on the shear plane. Earlier authors suggested that mantle-derived fluids may migrate through the SAF into the brittle portion of the crust (e.g. Kennedy et al. 1997), or that lateral flow of crustal fluids released from metamorphic processes penetrates the fault (Irwin and Barnes 1975), thereby contributing to fault-weakening high fluid pressures (Rice 1992; Kennedy et al. 1997, e.g.) and supporting fault creep (Figure 4c).

Alternatively, or additionally, serpentinite has been suggested as a possible cause for fault creep, because of its spatial close association with creeping faults in

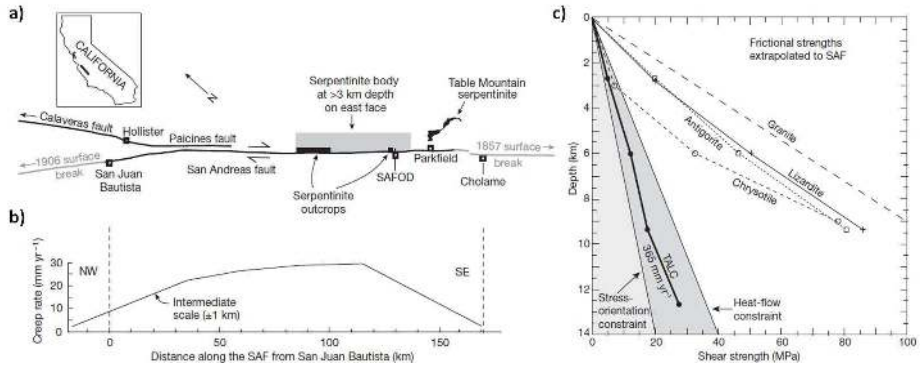

Fig. 3 The potential role of serpentinite for fault creep. **a)** Spatial association of serpentinite occurrences along the creeping SAF between San Juan Bautista and Parkfield-Cholame and **b)** correpsonding creep rates. **c)** Shear strength of talc and other minerals vs. depth (i.e. pressure). Only talc may account for the inferred low frictional weakness, constrained by stress orientations observed in SAFOD and by the absence frictional heat generation. Figures from Moore and Rymer (2007).

central and northern California (Figure 3a). However, serpentinite minerals do not exhibit shear strengths weak enough to account for fault creep. Moore and Rymer (2007) identified talc-filled shears and veins from cuttings of the SAFOD borehole and suggested that interconnected films of talc would only require small volume fractions to attain the observed frictional weakness. Talc, derived as reaction product from silica-saturated hydrothermal fluids with serpentinite, is frictionally weak over wide pressure and temperature ranges (Figure 3b), and thereby creates an indirect association between serpentinite and fault creep.

Because the veins and shears with which talc was found associated at SAFOD overprint all other textural features in the serpentinite grains, Moore and Rymer (2007) proposed that the talc is of recent origin. The decomposition of serpentinite with silica-saturated fluids (possibly derived from a deeper fluid source) to talc is a dehydration reaction and releases additional water into the system . However,

talc is only a minor constituent of fault zone rocks ($\sim 0.1\,\%$), and the generated fluid volumes are probably too small to influence the mechanical behavior of the fault directly. However, the presence of recently formed talc is an indication for fluid influx (transporting dissolved silica) into the fault system as well for active dehydration processes occuring in the crust. Therefore, it seems that explanations for fault creep involving serpenitinite (or talc) imply fluid circulation within the fault zone, and could be closely related or act in combination with high-pressure fluids.

2.3 The Fault Zone conductor

Conceptual fault zone models involving high-pressure fluids motivated MT studies to investigate the fluid distribution within and surrounding the fault zone. Early MT studies at Parkfield (Eberhart-Philips et al. 1995), in combination with seismic tomography, and at Carrizo Plain (Mackie et al. 1997) were able to discriminate some major geological units of the SAF system in terms of their electrical properties. In particular, the MT models at Parkfield revealed a broad upper crustal high-conductivity zone NE of the SAF, coincident with a seismic low-velocity zone. This zone was related to high-pore pressure brines, and Eberhart-Philips et al. (1995) speculated that fluids could be forced from the Coalinga anticline region in the NE to Middle Mountain, a push-up structure centered on the SAF near the SAFOD. Such a model was consistent with earlier fault zone models (Irwin and Barnes 1975; Eberhart-Philips et al. 1995) predicting that fluids released by metamorphic reactions within the Franciscan formation infiltrate the SAF and generate localized zones of high fluid pressure (Irwin and Barnes 1975; Rice 1992).

A different situation was encountered at Carrizo Plain, where the upper and middle crust east of the SAF appeared overly resistive, in contrast to simple geological models which juxtapose resistive Salinia against presumably more conductive Franciscan formation rocks along the SAF (Mackie et al. 1997). Both investigations at Parkfield and Carrizo Plain utilized spatial sampling distances of 5 kms on average, too coarse to resolve electrical structure related to the internal architecture of the SAF (Figure 5b).

High-resolution MT studies across the SAF with continous electric field profiling in its central parts revealed a more detailed electrical image of the SAF at Parkfield (Unsworth et al. 1997, 2000; Unsworth and Bedrosian 2004) and Carrizo Plain (Unsworth et al. 1999) and, later, at Hollister (Bedrosian et al. 2004). All of these studies imaged the upper few kilometers of the fault-surrounding crust. The most prominent feature of these models is a wedge-shaped high-conductivity zone above (Parkfield) or adjacent (Hollister) to the seismically defined fault (Figure 4). Elevated conductivities surrounding the uppermost portion of the fault were also imaged at Carrizo plain, though as a less pronounced feature of the resistivity model (Figure 5a). Such a fault-zone conductor (FZC), prominently apparent at Parkfield and Hollister, and modest at Carrizo Plain, is believed to correspond to saline fluid circulation within the damage zone of the fault and appears to be typical for the SAF and for many other faults worldwide (Ritter et al. 2005; Hoffmann-Rothe et al. 2004).

It is believed that the FZC is more or less continously associated with the SAF, at least where it exhibits creep. It has been imaged at two parallel profiles at Hollister and three parallel profiles at Parkfield, suggesting that it is regional

and not a local feature. A forth dense MT profile measured south of Parkfield is, as to my knowledge, unpublished. One profile was measured at Carrizo Plain.

Salinities measured in water wells at Parkfield (Hollister) require upper porosity bounds of 9-30 % (15-35 %) to account for the observed conductivity within the upper 2-3 kilometers of the fault, based on Archie's law (Bedrosian et al. 2004; Unsworth and Bedrosian 2004). At both locations, the FZC coincides with zones of reduced seismic compressional wave velocity (v_p) and enhanced v_p/v_s ratios (where v_s is the shear-wave velocity), consistent with a fluid-filled porosity network (Thurber et al. 2004, e.g.). Fluid filled voids and fractures are thus interpreted to represent the brecciated and damaged zone of the fault (Caine et al. 1996).

At the SAF, the width and depth extent of the FZC is developed variable along strike. At Hollister, where the fault creeps at high rates, the anomalous zone of high conductivity comprises several pockets of high conductivity between the San Andreas and Calaveras faults, and extends to mid-crustal depths beneath the SAF (Bedrosian et al. 2004) (Fig. 4a). At Parkfield, at the transition from fault creep to fault lock, anomalous conductivity is confined to a zone centred on the SAF and extending from the surface to a depth of 2-5 km (Fig. 4b), depending on location (Unsworth et al. 2000). In contrast, the FZC at the seismically quiescent SAF at Carrizo Plain is only weakly expressed, both in terms of conductivity and depth extent (Fig. 5a).

Along-strike variations of the FZC, with the more active fault segments associated with wider, deeper and more conductive FZCs, provide some insight how the FZC developed. In a detailed comparative study, Ritter et al. (2005) address the interplay between the extent and conductivity of the FZC, lithology, fluid supply, permeability and fault geometry. They proposed that the extent of the FZC along

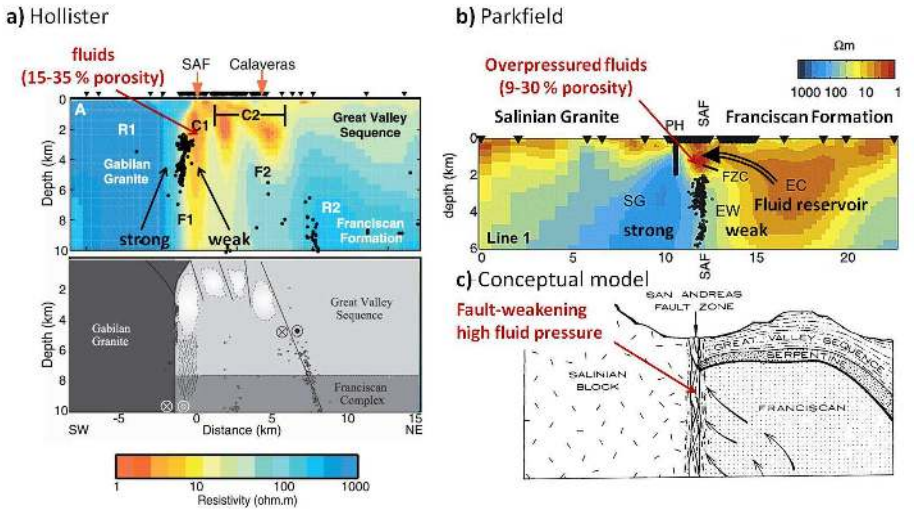

Fig. 4 Upper crustal resistivity models obtained from 2D inversion of profile MT data **a)** near Hollister (modifed after Bedrosian et al. 2004 **b)** near Parkfield (modified after Unsworth and Bedrosian 2004) and **c)** The magnitude of the fault zone conductor (FZC), believed to characterize saline fluids circulating within the damage zone of the fault, is variable along strike and correlates with the fault activity (e.g. Unsworth et al. (1999); Ritter et al. (2005)). **c)** Conceptual fault zone model of the SAF where it exhibits creep, modified after Irwin and Barnes (1975). Fluids, released by metamorphic reactions within the Franciscan formation and kept at high pressure below an impermeable layer (Serpentinite or layers of the Great Valley sequence) are believed to migrate laterally into the fault zone, contribute to fault-weakening high fluid pressures and thereby reduce shear strength.

the SAF reflects repeated episodes of healing, strength reloading and subsequent failure, causing the formation of broad zones of structural deformation. They further mention that a prominent strength contrast across the fault may result in deformation zones which effects the weaker, eastern block over a wider range. This seems to characterize the fault from top to mid-crustal levels near Hollister, and at Parkfield below the FZC.

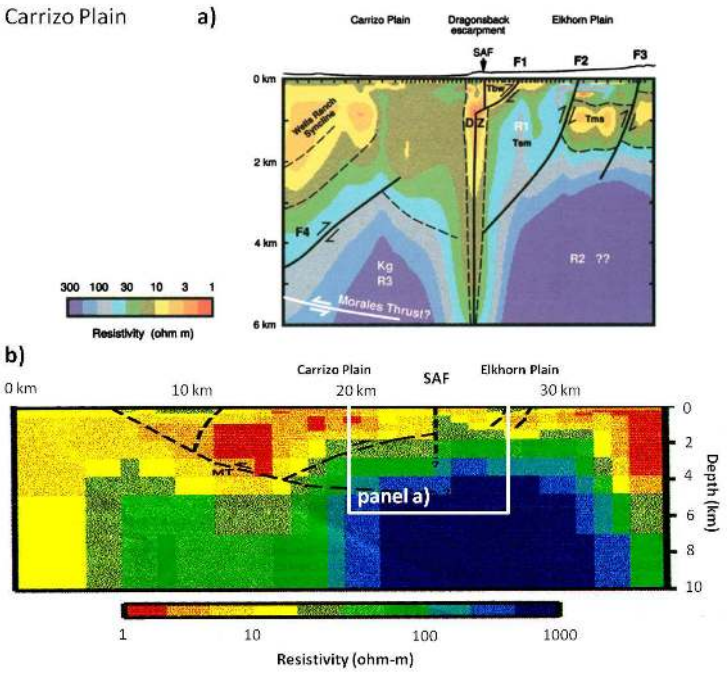

Fig. 5 Resistivity structure at Carrizo Plain. **a)** High-resolution study imaged a modest FZC, much lesser in magnitude than observed at the creeping segments near Parkfield Hollister (Unsworth et al. 1999). **b)** Upper crustal resistivity structure, showing a competent resistive block beneath and east of the SAF (Mackie et al. 1997). Black rectangle outlines model section shown in panel a.

Highly damaged rocks within the San Andreas fault zone at Parkfield form a low-velocity waveguide for seismic waves, giving rise to fault-guided wave propagation (Eberhart-Philips et al. 1995). Using surface and borehole seismic observations, Li and Malin (2008) estimate that a low-velocity waveguide along the fault at SAFOD extends at least to depths of ∼7 km and constitutes of a 30-40 m wide low-velocity fault-core embedded in a 100-200 m wide damage zone. The waveguide coincides with the FZC in its upper portion, but can be traced to greater depths. Increasing confining pressure with depth results in reduced porosity (compaction),

increasing seismic velocities within the waveguide, and, in conjunction with possible changes of the fluid composition, higher resistivities when compared to the FZC residing within the upper 2-3 kms. Even though resistivities associated with the fault core and damage zone at greater depth may still be lowered relative to the surrounding material, as seismic velocities are lowered within the waveguide, the deeper anomalous zone is probably too narrow to be resolvable with MT.

2.4 Seismicity-resistivity correlation

It is an intriguing observation that the regions characterized by FZCs are to a large extent devoid of microseismicity. Ritter et al. (2005) pointed out that the spatial relationship between the seismically defined active shear plan and the damage zone of the fault characterized by the FZC sheds some light on the dynamics of faulting.

At Parkfield, onset of seismicity is at $2-5\,\mathrm{km}$ depth, coincident with the base of the FZC. Below the FZC, seismicity is localized between resistive Salinian basement on the Pacific plate and more conductive rocks comprising Franciscan formation and sediments of the GVS on the North American plate. At Hollister, the upper $2\,\mathrm{km}$, corresponding to the zone of highest conductivity, are also devoid of seismicity, and seismicity associated with the SAF marks the western margin of the deeper parts of the FZC. Onset of seismicity along the Calavares fault near Hollister is at $\sim 5\,\mathrm{km}$ depth and correlates with a sharp increase of resistivity with depth; the connection between the seismically defined Calavares fault and its surface trace penetrates through conductive material and exhibits only minor seismicity (Fig. 4)

Absence of seismicity was used to suggest that the fluid-saturated fault breccias composing the FZCs are too weak to accumulate the shear stresses necessary to undergo brittle failure (Unsworth et al. 2000), provided that fluids are at hydrostatic pressure and hydraulically interconnected (Ritter et al. 2005). In turn, a sharp resistivity contrast across the western edge of the FZCs suggests that the fault is impermable for cross-fault fluid flow at deeper levels (Bedrosian et al. 2004; Ritter et al. 2005), in agreement with the onset of seismicity and with little geochemical evidence for fluid mixing across the fault. Because fluids at hydrostatic pressure tend to inhibit seismicity and overpressured fluids tend to induce seismicity, the spatial relationship beween the FZC and seismicity helps to characterize fluid pressure and permeability distribution within and surrounding the fault.

Fluid induced seismicity is not specific to the SAF but is also known on a larger scale and from deeper crustal levels. Gürer and Bayrak (2007) compiled a comprehensive catalogue describing the spatial relationship between electrically conductive zones and the distribution of seismicity for a number of tectonically active zones world wide. In general, fluid induced seismicity involves high-pressure fluids (sourced in conductive zones) invading rheologically strong (and resistive) formations, thereby facilitating mechanical failure and actively triggering seismicity or earthquakes within critically stressed regions (Jiracek et al. 2007).

Microseismicity along the SAF appears to localize in zones which exhibit a lithological contrast associated with a lateral conductivity gradient or contrast on a kilometer scale, from strong, resistive rocks to weak, conductive material (cf. Fig. 4). Superimposed on this kilometer scale trend is the actually deforming fault. SAFOD observation of the actively deforming fault strands have shown that the fault core (localized on a meter scale) is considerably weaker than its wall

rocks. This does, however, not imply that the weak SAF originally developed in a rheological gradient or contrast zone, because the western Salinian block has been displaced along a (pre-existing) fault to its present position. Nethertheless, the inferred rheological heterogeneities surrounding the fault zone may affect present deformation, and should be used to better constrain mechanical models, which are frequently based on layered-earth background rheology models (e.g. Chéry et al. 2004).

2.5 Crustal fluid source and indications for mantle-derived fluids

The source of fluids circulating in the damage zone, and in formations surrounding the fault, is probably multifold. In addition to fluids of meteoric origin, with a maximum circulation depth of $\sim$ 6 km (Kharaka et al. 1999) estimated on the basis of geochemical signatures of spring and well fluids, Irwin and Barnes (1975) suggested that fluids emanate from metamorphic reactions within the Franciscan complex. These fluids could be transported laterally into the fault zone, because they are capped by impermeable layers of the Great Valley sequence or a layer of serpentinite (cf. conceptual model in Fig. 4c). Geochemical studies of fault-zone materials by (Pili et al. 1998) support this conclusion and suggest that during deformation the fault zone is infiltrated by mixed H_2O-CO_2 fluids of metamorphic or deep crustal origin. Finally, a locally high flux of mantle-derived fluids is inferred by Kennedy et al. (1997) based on helium isotopic ratios in springs and seeps along the SAF.

Kennedy et al. (1997) proposed that a permeable fault or damage zone surrounded by low-permeability country rock may act as a conduit for mantle-derived

fluids and allow for large fluid pressures to be localized within the fault zone (Rice 1992). They argued that mantle fluids passing through the ductile lower crust must enter the brittle fault zone at or near lithostatic pressures and suggested that they may thus contribute directly to fault-weakening high-fluid pressures at seismogenic depths.

However, SAFOD observations, including contrasts in both fluid chemistry and fluid pressure across the fault zone, suggest that rather than acting as a permeable conduit, the fault appears to be considerably less permeable than the surrounding crust and acts as a barrier for both vertical and horizontal fluid flow (Zoback et al. 2006). This would be in agreement with a sharp resistivity contrast across the seismically defined fault, as observed near Hollister and, at depths below the FZC, near Parkfield (Figure 4). Furthermore, SAFOD provided no evidence for near-lithostatic fluid pressures within the fault core. Zoback et al. (2010) thus concluded that high fluid pressures are not the primary cause for the apparent weakness of the fault.

However, observations at the depth of the SAFOD borehole may not fully reflect the fluid pressure state within the fault zone over much of its depth extent. It can therefore not be precluded that the fault is permeable at deeper or shallower levels, that substantially higher fluid pressures exist within deeper portions of the fault (Fulton and Saffer 2009), or that dynamic fluid pressure-buildup and pressure release associated with the seismic cycle occurs. However, dynamic changes related to the fluid budget would probably have a minor effect on bulk electrical resistivity, because telluric and MT monitoring did not detect any resistivity changes which could be associated with the Parkfield M6.0 earthquake (Park et al. 2007; Kappler et al. 2010).

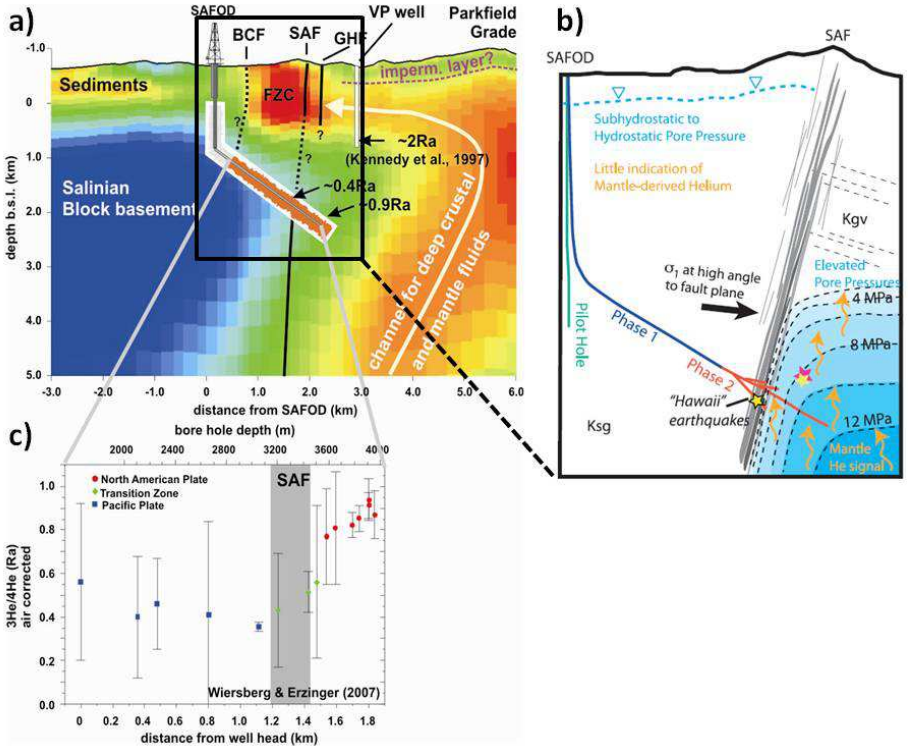

Fig. 6 Scenario for fluid distribution in the vicinity of the SAFOD, with influx from mantle-derived fluids. **a)** Resistivity model across the SAFOD (Becken et al. 2008), coincident with line 1 of Unsworth and Bedrosian (2004) shown in Figure 4a. **b)** Predicted fluid pressure distribution in the North American Plate due to dehydration of a serpentinzed mantle wedge (Fulton and Saffer 2009), which is consistent with SAFOD observations. **c)** A profile of 3He/4He ratios across the SAF indicates increased mantle-derived gas concentration within the North American plate (Wiersberg and Erzinger 2007), consistent with earlier He isotope studies in the Varian Philipps (VP) water well (Kennedy et al. 1997). Suprahydrostatic fluid pressures within the North American Plate, He isotope studies and the MT resistivity model agree in suggesting that pathways for deep fluids exist into the North-American plate, and that fluids are trapped between an impermeable SAF and an impermeable near-surface layer.

It has furthermore been observed that fluid pressures and mantle-derived gas concentrations are elevated within the fault-adjacent country rock of the North American plate. Additionally, geochemical signatures of mud gas, logged while drilling the SAFOD (Wiersberg and Erzinger 2007), revealed a positive mantle-derived gas-concentrations gradient away from the SAF into the North American plate, suggesting that pathways exist adjacent to the fault and that deeply sourced fluids may percolate into the eastern fault block.

The upper crustal lithology east of the SAF near Parkfield comprises both sediments from the Great Valley Sequence and Franciscan Formation. Within this geology, a pronounced zone of high electrical conductivities (Eberhart-Philips et al. 1995; Unsworth and Bedrosian 2004; Becken et al. 2008), coincident with a region of lowered velocities (Thurber et al. 2004), may represent the source or a trap for crustal and mantle-derived fluids which are speculated to penetrate the fault zone laterally from the east (Unsworth and Bedrosian 2004). This zone is referred to as the eastern conductor (EC). In this region, a 2 km deep layer of magnetic serpentinite is interpreted from potential field data (McPhee et al. 2004), however, remains unconfirmed from MT data (Unsworth and Bedrosian 2004). Such a layer of serpentinite, or layers of the GVS, could act as an impermeable seal, as suggested by Irwin and Barnes (1975), give rise to overpressured fluids within the reservoir below and consequently drive fluids laterally towards the fault zone.

Lateral fluid flow from the east into the fault requires open pathways between the EC and the seismically-defined fault itself. The geometry of these pathways, if existing, is however, not clear. Seismic joint v_p, v_s and $v_p v_p/v_s$ inversion (Zhang et al. 2009) and seismic attenuation tomography (Bennington et al. 2008) consistently infer a fault-adjacent near-vertical zone that is characterized by high v_p/v_s

ratios and low attenuation. This anomalous zone easterly adjacent to the fault extends below $\sim$ 1 km depth, is less than 1 km wide, separates the FZC region (characterized by low resistivity and low velocity) from the EC, and appears to coincide with a sliver of GVS sediments (cf. Figure 7f in Zhang et al. 2009). Its seismic properties are indicative of a low-porosity zone and do not support the previous MT interpretations of fluid pathways into the FZC at these depth levels (Unsworth and Bedrosian 2004). Potential fluid flow into the FZC is therefore more likely concentrated at shallower levels, coincident with the zone of highest conductivities in the upper 1 km (cf. sketched fluid path in Figure 6a), and possibly at deeper levels.

The situation may be different at Hollister, where Great Valley sequence sediments are based by moderately resistive Franciscan Formation at 6-8 km depth, and where a fluid source or reservoir within the fault-adjacent rocks appears absent. If crustal fluids derived from metamorphic reactions within the Franciscan formation, or fluids of deeper origin, contribute significantly to the fluid budget of the SAF at Hollister, they would possibly migrate along near-vertical pathways easterly adjacent to the SAF, where high conductivities are encountered to mid-crustal levels. At Carrizo Plain, no indications have been found for deeply penetrating conductor zones. Here, the crust appears overly resistive to mid-crustal levels, suggesting that fluid influx from the lower crust or deeper is absent. However, regional scale MT studies which could test for the presence or absence of crustal scale conductive zones, are missing from both locations, Hollister and Carrizo Plain.

In summary, SAFOD observations and MT resistivity studies near Parkfield consistently infer deeply rooted fluid pathways into the eastern fault block. Conse-

quently, these results strongly support the existence of a deeper fluid source and at least episodically open pathways for fluids migrating into the brittle regime. However, it remains a debated question, if and how these fluids control the mechanical state of the seismogenic fault.

2.6 Crustal fluid pathways

A crustal MT study across the SAF at the SAFOD showed that the Eastern Conductor (EC) inferred to be a fluid reservoir or trap for crustal and mantle-derived fluids is rooted in the lower crust or deeper (Figure 7a). This near-vertical zone of high conductivities, appearing uninterupted from the near surface east of the fault across the SAF at mid-crustal levels and broadening beneath the SAF into the lower crust, has accordingly been interpreted in terms of a channel for deep fluids into the seismogenic zone (Becken et al. 2008). If explained with interconnected pathways for fluids, and fluid upflow across the entire crust, this conductive channel is consistent with many of the surface and SAFOD observations mentioned above.

Superimposed on the resistivity model in Figure 7a are structural interpretations from a seismic reflection and refraction survey (Hole et al. 2004; Ryberg et al. 2005; Bleibinhaus et al. 2007; Buske et al. 2007), which show good agreement with resistivity structure. On the Pacific plate, the Salinian block basement is based by a layer with lowered velocity, interpreted as metasedimentary rocks, and coincident with lowered resistivities here. A near-vertical fault zone (F) imaged with Fresnel-volume-migration (Buske et al. 2007) could correspond to the deep-reaching lateral resistivity contrast at the transition to the Salinian block

to the west. An active thrust fault east of the fault that abuts the SAF at the base of the seismogenic zone has been proposed near the edge of the upper crustal high conductivity zone in the upper crustal eastern fault block (EC), based on the analysis of earthquake data (dashed line T in Fig. 7a). The reflector element H (Bleibinhaus et al. 2007) may represent a lower crustal continuation of this thrust.

High-conductivity zones imaged with MT near SAFOD appear in spatial close association with the occurrence of serpentinite, and could be causally or indirectly related. Evidence for widespread serpentinite occurence comes from nearby outcrops, in combination with aeromagnetic interpretation, and serpentinite and talc findings within SAFOD (cf. section 2.2). Serpentinite originates from ultramafic mantle rocks which have been altered by hydration. Serpentinite is weaker than unaltered mantle peridotie, exhibits more viscous mechanical properties and lower density. Due to its bouyancy under high confining pressures at depth, serpentinite is prone to exhumation through weak zones in the crust. Kirby et al. (2002) suggested that a serpentinized mantle wedge, relic from ceased Farallon subduction, may be a deep source region for serpentinite slivers that occur along the SAF. If this was the case, it would be possible that remnants of serpentinite exists also at deeper crustal levels.

A recent receiver function (RF) study supports the occurrence of serpentinite within the lower crust (Ozacar and Zandt 2010). Using data from a long-term seismological station (PKD) located 3 km SW of the SAF near SAFOD, Ozacar and Zandt (2010) found that RFs display strong polarity reversals that require strong seismic anisotropy in a low velocity, high v_p/v_s layer at $18 - 26\,\mathrm{km}$ depth, that has a ENE dipping rock fabric (Figure 7b). The authors suggested that serpentinite at lower crustal pressure conditions could exhibit the modelled low velocity

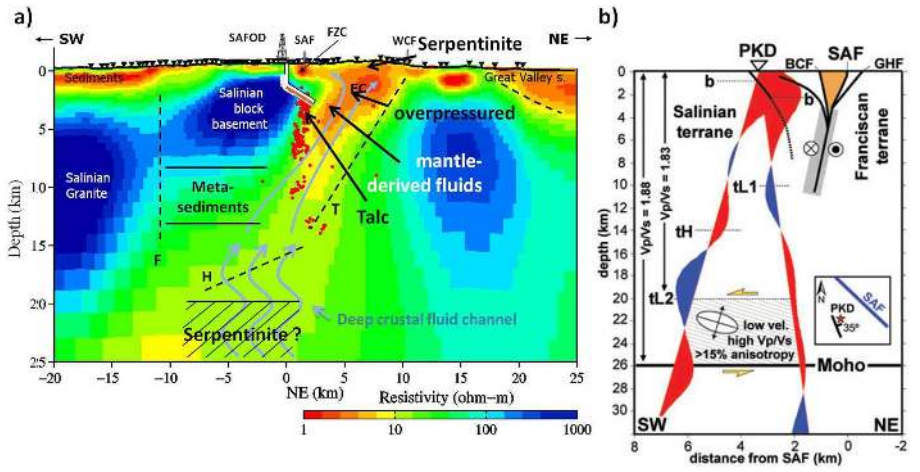

Fig. 7 Crustal structure at SAFOD. **a)** Interpreted MT resistivity model. High electrical conductivities appear uniterrupted from the EC into the lower crust or deeper, and have been proposed to represent pathways for fluids (Becken et al. 2008), consistent with elevated fluid pressures and mantle derived fluid concentrations in the eastern fault block. A seismic low-velocity layer below the resistor denoted as the Salinian block basement, and a reflector element (H) have been interpreted from a seismic reflection experiment (Bleibinhaus et al. 2007). T may represent a thrust fault (Carena 2006), bounding the zone of highest electrical conductivities to the east. F indicates a fault zone illuminated by Fresnel-volume-migration of the same seismic data set (Buske et al. 2007). Red dots mark seismicity. **b)** Polarity reversal of receiver functions at station PKD located above the Salinian block have been modelled with an anisotropic layer, possibly corresponding to serpentinite (Ozacar and Zandt 2010). I propose that the zone imaged as electrically conductive may correspond to the exhumation path for serpentinite (see text).

and high v_p/v_s ratio simultaneously; other rocks types are typically faster or have lower v_p/v_s ratios, even if fluid bearing. The orientation of ENE anisotropic fabric of this layer, dipping at only 35°, is inconsistent with the San Andreas sense of shear. Therefore, Ozacar and Zandt (2010) explained the anisotropic layer with a

fossilized fabric of past eastward-directed (Farallon Plate) subduction, maintained in serpentinite rocks.

RFs place the presumed serpentinite layer at the base of the crust to the southwest of the seismically defined SAF, probably owing to position of the PKD site west of the fault. However, a serpentinite sliver at depth located west of the fault trace would be in geometrical agreement with on overall SW dipping geometry of the crustal conductor inferred to represent pathways for fluids.

Based on the coincidence of conductive zones and serpentinite at different crustal levels, we hypothesize that the crustal conductive zone coincides with a region occupied by serpentinite slivers, and fluid pathways are related to the crustal exhumation path of serpentinite. Fluids (episodically) migrating along these pathways could contribute to elevated fluid pressures and explain elevated mantle-derived gas observed within the SAFOD on the North American plate (Wiersberg and Erzinger 2007) and within nearby water wells (Kennedy et al. 1997; Zoback et al. 2006), and could furthermore provide dissolved silica reacting with emplaced serpentinite to talc (Moore and Rymer 2007) (cf. section 2.2).

If high conductivity and the occurence of serpentinite are indirectly related through painting common pathways for fluids and serpentinite exhumation, and if RFs can probe for serpentinite at lower crustal levels, as proposed by Ozacar and Zandt (2010), then the combination of MT and RF analysis could be useful to determine systematic variations of crustal conductive zones, serpentinite occurence at depth and their relationship to the mechanical state of the fault. Unfortunately, the PKD station is the only station nearby Parkfield, which provided long enough recordings to apply this analysis (Ozacar, personal communication).

2.7 Fluid migration across the brittle-ductile transition zone

Fluid flow through rocks at different crustal and upper mantle depths has received considerable attention during the last decade. In general fluids are driven upward owing to buoyancy forces acting on low-density fluids. However, upward crustal fluid flow may become arrested at mid-crustal levels, and uniterrupted fluid pathways across mid-crustal levels seem to be the exception rather than the rule. Different mechanisms and model are invoked to explain fluid flow and fluid arrest. Understanding fluid flow patterns from a thermomechanical perspective is beyond the scope of this paper. However, as it is anticipated that mantle-derived fluids percolate into upper crustal fault blocks, these issues must be addressed. Therefore, we briefly summarize some aspects of fluid flow through the crustal levels.

According to modern thermomechanical models, under compressional conditions even initially pervasive pore fluids are mechanically unstable and must form focused flows whose shape depends on the relations of fluid and lithostatic pressures (Connolly and Podladchikov 2004, e.g.). Porosity waves are one of the possible mechanisms for both segregation and trapping of fluids released by diagenetic and metamorphic reactions. Ascending buoyant fluids are envisaged as percolating upward through an interconnected fluid-filled porosity network. Flow can become pulsed in zones of high porosity, may grow by draining fluid from the background porosity and leave a wake of elevated porosity that localizes subsequent flow (Aranovich et al. 2009).

Porosity waves may be stalled below a high-strength layer or in stagnant zones of tectonically induced neutral buoyancy (Connolly and Podladchikov 2004). These

mechanisms can result in the formation of high-pressure fluid reservoirs below the transition between the brittle and ductile portions of the crust. Jiracek et al. (2007) explore these concepts to address the question how earthquake rupture in the brittle crust is initiated by permeable, overpressured fluidized zones in the ductile crust. Evidence for the existence of stalled fluids (both melts and aqueous fluids) below the brittle-ductile (BD) transition zones comes from MT studies around the world, which frequently imaged lower crustal high-conductivity with clear depth to their top below the BD transition or deeper.

The situation seems to be different at the SAF near SAFOD, where a subvertical zone of high-conductivities occurs in the ductile crust beneath the San Andreas fault and appears to continue uninterrupted to the near-surface. Comparing these results with MT models from the Himalaya and from New Zealand, (Jiracek et al. 2007) pointed out that untapped and continously rising fluids may faciliate weaker but more frequent earthquakes compared to the Southern Alps in New Zealand and the Himalaya. They suggested that low convergence characterizing the Coast Ranges in Central California rates may not allow the formation of stalled fluid reservoirs in stagnant regions of neutral buoyancy or at permeability or strength contrast, because their formation is favoured in compressional settings.

In addition to these explanantions, we note that the crustal conductive zone has oblique, apparently westward dipping geometry, and breaches the BD transition zone at the base of seismically defined fault. As pointed out previously, the SAF is an extremely weak zone, is associated with stress rotation, and may perturb the depth range of tectonically induced neutral bouyancy or even prevent its formation in its vicinity. Thus, the concept of fluid stallation and the formation of high-pressure regions at mid-crustal levels may not be applicable to the particular,

highly heterogeneous situation at the SAF near the SAFOD, and continously or episodically open pathways for fluids across the BD transition do not contradict the concept of neutral buoyancy in general.

Furthermore, as we shall see later, a high-conductivity zone with its top clearly located below the BD transition was found beneath the Coast Ranges, offset from the SAF to the west, and could indeed correspond to stalled fluids as promoted by the concept of tectonically induced neutral buoyancy.

3 The deeper roots of the SAF, fluid sources and geodynamic implications

The deeper roots are less amenable to direct observation of fault activity, and different models for the deep roots of fault zones such as the SAF have been proposed. Endmember models include distributed upper crustal strain rooted in a broad ductile shear zones, singular through-going faults, or upper crustal faults connected via mid-crustal decollements, and have been discussed in Ritter et al. (2005).

Tectonic 'non-volcanic' tremor (NVT), a recently discovered seismic signal (Nadeau and Dolenc 2005) is believed to provide new insight into the geometry and physical conditions of the deep roots of faults. NVT observations at the SAF system are confined to a small number of source regions, probably limited by detection threshold. Highest tremor activity is observed near Cholame, at the northern end of the zone that was ruptured by the Fort Tejon earthquake in 1857 (Nadeau and Dolenc 2005). Because the nucleation of tremor is believed to be intimately related to fluids, we start the discussion of the deeper roots of the SAF

with recent NVT observations. We will then expand the discussion on results from a regional scale MT survey in the tremor source region, and consider implications for the geodynamic setting.

3.1 Non-volcanic tremor

Accurate localization of tremor is generally difficult because of the absence of a sharp onset of seismic energy for this family of signals. Most authors have located tremor vertically beneath the SAF at depths greater than 25 km (Nadeau and Dolenc 2005; Shelly et al. 2009). The localization techniques used by these authors estimate tremor sources relative to some master event, which yields high relative localization acuracy, but may be biased due to inaccuracies in the master event position. Alternative location estimates are based on analysis of data from so-called small seismic aperture arrays (SSAA), which determine absolute source positions for each individual termor episode. Using this approach, Ryberg et al. (2010) determined source locations at slightly greater depths (30-50 km) and systematically offset from the SAF by 15-20 km. Epicenters estimated with both techniques are indicated on the map in Figure 8. To match the source locations of Shelly et al. (2009), a calibration technqiue was applied to the SSAA estimates. However, the discrepancies show that there remains some uncertainty about the exact source region of tremor near Cholame.

Tremor sources are not static but can be shown to migrate along the fault with velocities in the range 17-80 km/h. Tremor has been observed to migrate up to 25 km along the fault, though most of the observed episodes travel by 5-10 km (Shelly 2010). Detailed inspection of along-strike tremor migration episodes has

been used to suggest that the fault exists as a (piecewise) continuous structure at the 25 km depth of the investigated tremor families (Shelly 2010).

The source mechanism of NVT is not well understood. High pore-fluid pressures, released by dehydration reactions in the subducting plate, have been suggested to promote the nucleation of deep non-volcanic tremor, low-frequency earthquakes and slow-slip at the Cascadia subduction zone (Schwartz and Rokosky 2007) and in Japan (Shelly et al. 2006). In subduction zones, these seismic phenomena appear to represent a mode of failure along the subducted plate interface between the locked megathrust updip and the continuously creeping zone downdip (Obara 2002, e.g.).

Teleseismic triggering of tidal forcing of NVT at the SAF near Cholame and at other locations indicates that the deep fault is extremely sensitive to small stress perturbations. This suggests the presence of high, near-lithostatic fluid pressures in a critically stressed source region (Thomas et al. 2009), similar to the physcial conditions proposed for subduction zone tremor. High fluid pressures may make the fault extremely weak, possibly permitting patches of the deep fault to deform by brittle rather than ductile failure, and support localized slip on the deep extension of the SAF (Shelly 2010). Localized deformation in the ductile deformation region is possible where strain softening occurs and water-weakening is one mechanism to facilitate this (Jiracek et al. 2007). Thus, tremor occurrences provide several indirect indications for the existence of a fluid source at tremor source depth.

The nature of the fault between the base of the seismically defined fault ($\sim$ 15 km) and the onset of tremor ($\sim$ 24 km, or deeper), however, is unknown, as this area is devoid of earthquakes and does not appear to generate appreciable tremor. (Nadeau and Dolenc 2005) found that changes in tremor and micro-

earthquake rates at Cholame appear to correlate. This suggests that deep deformation associated with the Cholame tremors may also be stressing the shallower seismogenic zone in this area. In turn, tremor rate and recurrence behaviour changes in the wake of the 2004 M6.0 Parkfield earthquake may reflect the effects of static and dynamic stresses imparted by the earthquake and influencing ongoing deep fault deformation. These examples show that tremor on the deep fault and seismicity and earthquakes on the upper crustal fault are processes that are coupled across lower and mid-crustal levels, suggesting that the fault is throughgoing.

3.2 High conductivity zone in the lower crust and upper mantle

A regional-scale MT array imaged crustal and upper mantle resistivity structure across the entire transitional Parkfield-Cholame segment of the SAF, from the Pacific coast into the central value. The resistivity models presented in Figure 10 (Becken et al. 2011) rely on 2D inversion techniques of seven individual profiles constituting the array (Figure 8a). These models indicate that the across-strike resistivity structure is not uniform along the SAF but exhibits significant along-strike variations. Because of this fact, the validity of a 2D approach may be questionend. Therefore, before discussing the resistivity models, I briefly summarize how 3D effects in the data were taken care off, and how the pseudo 3D model (i.e. stitched 2D models) was validated.

Multi-period single-site galvanic distortion and strike analysis (Becken and Burkhardt 2004) of the entire impedance data set yielded strike estimates strongly consistent with the general strike direction of the SAF and the lithological units forming the Coast Range geology (see inset in Figure 8a). Closer inspection of

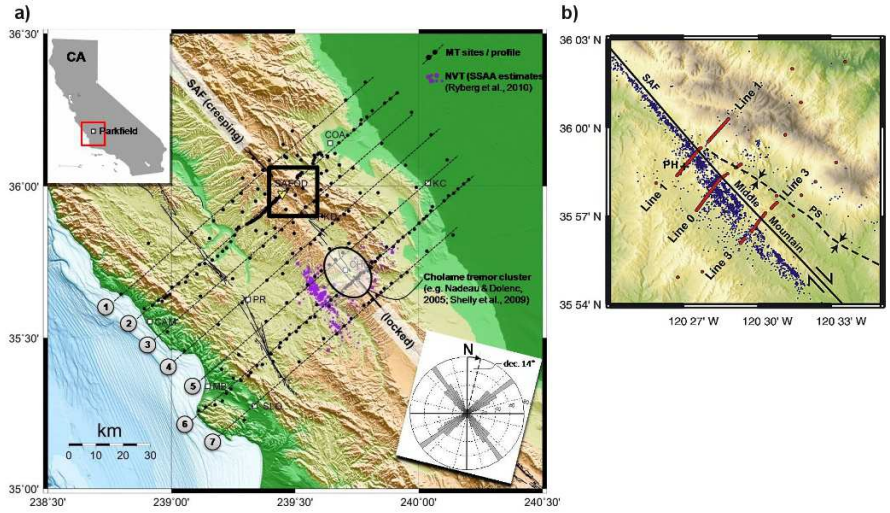

Fig. 8 MT sites probing upper mantle and crustal structure along the Parkfield-Cholame segment of the SAF in Central California. **a)** Regional-scale MT study (Becken et al. 2011) using seven 120-140 km long profiles. Black dots depict MT site locations. Rose diagram in the lower inset displays cumulative geoeletric strike estimates consistent with the geological strike of the SAF. Purple dots: NVT epicenter estimates based on the SSAA-technique (Ryberg et al. 2010); Shaded ellipse: outline of NVT epicenters, based on other localization techniques (Nadeau and Dolenc 2005; Shelly et al. 2009); Black rectangle: outline of the map section shown in right panel. **b)** High-resolution investigation of the SAF (Unsworth and Bedrosian 2004). Red dots indicate MT stations; blue dots show seismicity. PH SAFOD pilot hole; PS Parkfield syncline. An additional dense MT profile farther south is beyond the map extent.

the data revealed that 3D characteristics are minimized in this rotated coordinate system but do not vanish for a range of sites, indicating that the estimated strike direction is the dominant direction contained in the impedance data, but not necessarily a valid strike direction for all sites. Furthermore, the orientation of induction vectors deviates significantly from the strike-perpendicular profile directions. Therefore, data with obvious 3D effects were downweighted for 2D inversion

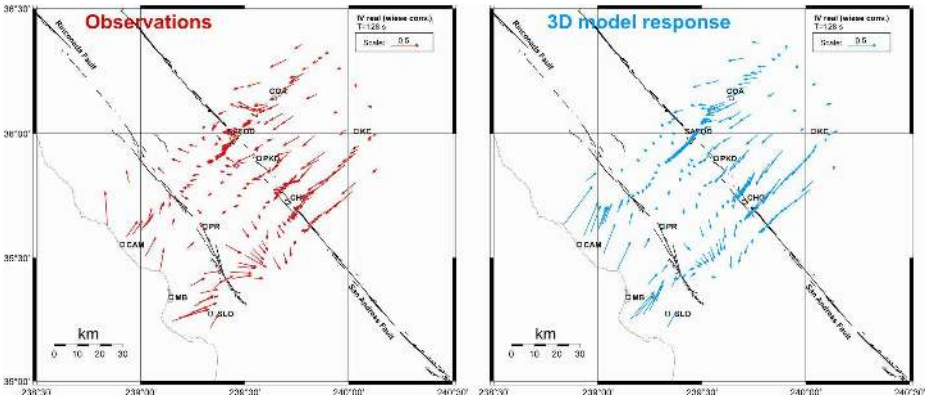

Fig. 9 Comparison of observed induction vectors (real parts, depicted in Wiese convention (Wiese 1962)) and 3D forward model response, based on inter- and extrapolation of 2D inversion models onto a 3D grid. Period is $T = 128\,\mathrm{s}$, corresponding to mid-to-lower crustal penetration depth. Figure from (Becken et al. 2011).

by imposing error bars in proportion to their departure from 2D characteristics, following the procedure discussed in Becken et al. (2008). This approach helped to avoid overfitting the data where they are afflicted with 3D effects.

To validate the models after 2D inversion, (Becken et al. 2011) computed model responses from a 3D model constructed by inter- and extrapolation of 2D models onto a 3D grid. Figure 9 compares 3D modelled with observed induction vectors for a period of $T = 128\,\mathrm{s}$, corresponding to crustal penetration depths where 3D effects are most prominent. This test shows that the 2D approach can reproduce the most important inductive 3D effects, suggesting that the along-strike variations encountered by 2D technqiues are, at least to some extend, real. Ultimately, 3D inversion will be required to translate all aspects of the 3D data into model structure, and will be presented in future (Tietze et al., 2010, reference missing).

Figure 10 shows 2D inversion results along profiles 1-7 in perspective view. Models have been truncated at the profile ends and at 60 km depth. Superimposed

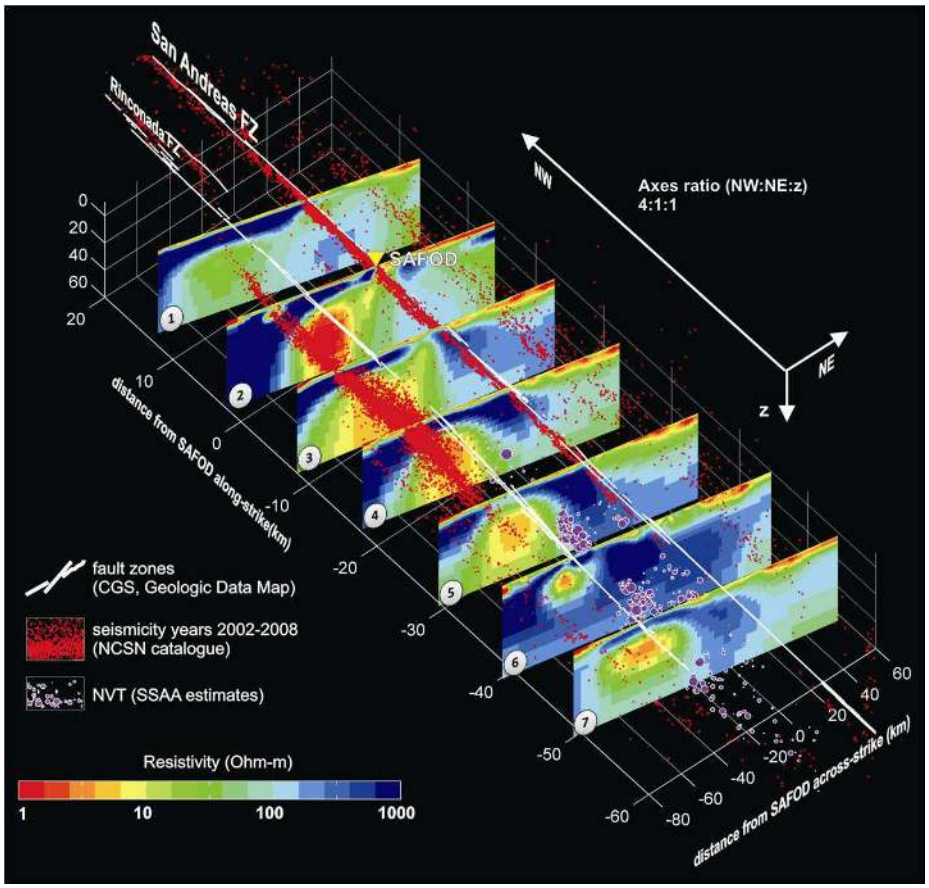

Fig. 10 Regional-scale resistivity structure across the Parkfield-Cholame segment of the SAF in Central California, obtained from two-dimensional inversion of seven individual $120-140$ km long profiles across the SAF. Model penetrate into the upper mantle and are truncated at ~ 60 km depth. (modified after Becken et al. 2011). A prominent high-conductivity zone centred at 20-30 km depth and locatde between the SAF and the coast is interepreted with hjydrothermal fluids residing within a ductile strain generated permeability structure. Crustal fluid pathways have been proposed account for the conductive crustal zone near the SAFOD, where the SAF is transitional-to-creeping. Farther south, where these pathways are absent, where the brittle fault is transitional-to-locked, and where non-volcanic tremor deep is observed at depths greater than 20 km, deep fluids may be trapped at high pressures.

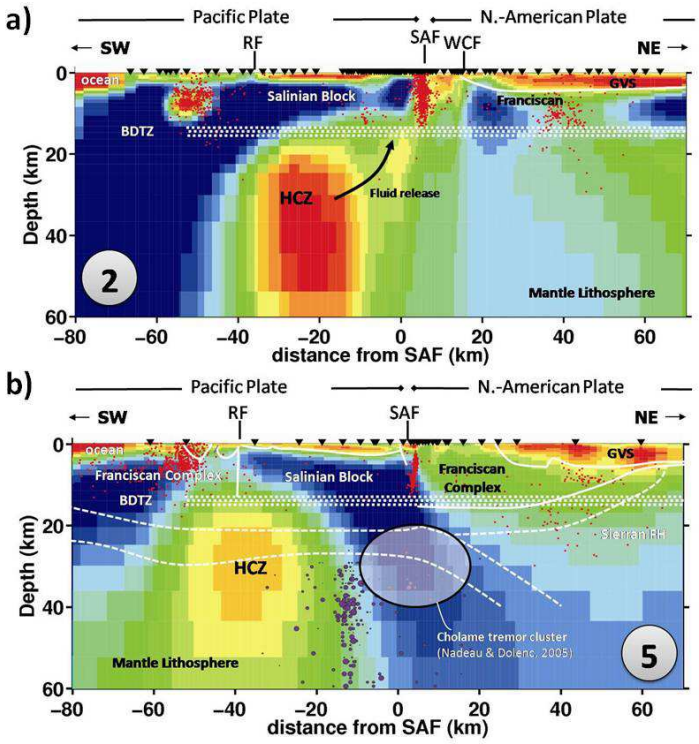

Fig. 11 Regional scale resistivity models across the SAF **a)** at SAFOD near Parkfiled **b)** at the source region of tremor near Cholame. Models are based on 2D inversion of profile data; the profiles are separated by ~ 30 km. Red dots mark seismicity, purple dots indicate NVT source estimates using the SSAA technqiue Ryberg et al. (2010), ellipse outlines source locations estimated with other technqiues. RF Rinconda fault; WCF Waltham canyon fault; HCZ High conductivity zone. BDTZ Brittle-ductile transition zone. Superimposed are geological units (white lines in panel b) from the coincident geological cross-section depicted in Figure 2. Figure from Becken et al. (2011).

on the models are the 3D distributions of seismicity (red dots) and NVT estimates (purple doots) based on the SSAA technique (Ryberg et al. 2010). Profiles 2 and 5 across the SAFOD and the source region of tremor, respectively, are shown in Figure 11.

The most prominent structure revealed by the MT data is a deep high-conductivity zone (HCZ, 1-5 ohm-m), centred 30-40 km southwest of the SAF below 20 kms depth and elongated in parallel to the SAF. Becken et al. (2011) proposed that mineralized fluids within a interconnected porosity network could account for the observed conductivties of the HCZ centered at 25-30 km depth between the SAF and the coast. Bulk rock conductivity of a multi-phase system is strongest depending on the conductivity of the most conductive phase and its interconnection. Aqueous fluid conductivity is controlled by electrolytic concentration and temperature. Modelling of the Coast Range Heat flow anomaly suggest temperatures of ~800°C at 30 km depth near Parkfield (Sass et al. 1997). At these temperatures the electrical conductivity of sea water is approximately ten times higher than at room temperatures (Quist and Marshall 1968). Fluids with a salinity comparable to that of sea water and at 800°C have a conductivity of 30 S/m. The Hashin-Shtrickman upper bound (Hashin and Shtrikman 1962) for a two-phase system composed of a resistive rock matrix (0.01 S/m) and a conductive fluid phase (30 S/m) requires 3 vol.% of perfectly interconnected porosity over a large volume to yield bulk conductivities of 1 S/m. A lower degree of pore interconnection would mean larger fluid volumes, which appear unrealistic at these depths. In turn, lower volumes of fluid would be required at the same high degree of interconnectivity if the temperature and/or the fluid conductivity were higher. Therefore, volumetric porosities as low as a few percent with pores interconnected over large scales are sufficient to explain the observed conductivities of the HCZ.

Different mechanisms may account for fluid interconnectivity in ductile regimes. These include fracture interconnectivity, grain-edge interconnectivity or both (Jiracek et al. 2007). In addition, peremability must be maintained over time, either by con-

tinous deformation, permeability-enhancing reactions or high fluid pressures, or a combination of these mechanisms (Jiracek et al. 2007; Cox 2005). Long-lasting deformation can generate interconnection on long distance ranges. A strain-generated and maintained porosity network could thus explain the degree of pore connectivity assumed by the Hashin-Shtrickman upper bound. Because the actively deforming transform margin migrated inland since its initiation, it is likely that a broad region has experienced strain during the evolution of the fault system. MT cannot distinguish between permeability structure in actively deforming zones and maintained permeability formed in previously active zones. Only small strain rates, perhaps in combination with other mechansims, are required to maintain permeability in a ductile deformation regime, once developed (Jiracek et al. 2007). Thus, the HCZ likely represents a ductile deformation region with maintained hydraulic permeability.

Note that the HCZ is offset from the SAF and located beneath the predominantly resistive crustal Salinain Block. The Salinian Block is rheologically strong and impermeable for fluid flow in the brittle crust. Below the BD transition, ductile deformation prevails. Under these circumstances, a stagnant zone of neutral buoyancy could have developed beneath the Salinian Block (at depths greater than the BD transition) in response to a regional transpressive stress regime and supported the formation of tabular water sills as suggested by Connolly and Podladchikov (2004) and described by Jiracek et al. (2007). Lateral fluid flow in a stagnant zone with small or vanishing vertical hydraulic gradient could be one of the means to drive fluids into the SAF farther to the east. At the SAF, perturbations in the stress state, associated for instance with a weak fault as outlined previously, could

result in perturbations of the stagnant zone and facilitate fluid flow further upward across the BD (cf. section 2.7).

Crustal structure surrounding the SAF exhibits significant along-strike variation, in intriguing correlation with the spatial pattern of upper crustal seismicity and deep non-volcanic tremor. Where the fault is transitional-to-creeping and characterized by microseismicity in the brittle crust, and where NVT is of lesser magnitude or absent, an overly conductive crust connects with the HCZ (Figs. 10 and 11a). In turn, where the fault is transitional-to-locked, where only minor microseismic activity is observed in the upper crust, and where the majority of NVT episodes is localized at depths corresponding to the HCZ, the crust is overly resistive between the SAF and the HCZ (Figs. 10 and 11a).

As outlined previously, the crustal conductive zone imaged near SAFOD, has been suggested to represent a channel for deeply rooted fluids into the seismogenic SAF (Becken et al. 2008). The regional scale MT data suggest that this crustal conductive zone connects directly with the HCZ at upper mantle depth and offset from the SAF trace to the southwest. This implies that the HCZ may correspond to the source region of mantle-derived fluids, which find pathways through crustal levels near SAFOD (Becken et al. 2008, 2011), and which are responsible for the elevated mantle-derived gas concentration and fluid pressures east of the fault. In turn, and if fluids are responsible for the HCZ, these fluids appear to be trapped to greater depths farther southeast along the SAF, where such crustal pathways are absent, where the fault transitions to mechanical lock and where NVT is observed.

3.3 Hydrated mantle wedge as the fluid source?

If fluids are responsible for the HCZ, it is a key issue is to address the source of these fluids. In subduction zones, the subducting slab is the obvious fluid source, either by direct dewatering in the early subduction stage, or by hydration-dehydration reactions with increasing slab depth and increasing temperatures and pressures (e.g. Wannamaker et al. 2010). Fluids released from the slab may percolate into the overlying mantle wedge, and farther into the lower crust, and account there for high conductivity anomalies. In addition, aqueos fluids may support the formation of partial melts, which are for instance believed to persist beneath the Altiplano Plateau and responsible for a widespread high-conductivity anomaly observed with MT (e.g. Schilling et al. 1997).

In Central California, no such obvious fluid source exists, because subduction terminated ~ 20 Ma ago. However, some authors have suggested that dehydration of a serpentinzed relic mantle wedge, formed during subduction along coastal California in a way analogous to modern subduction systems, may still release fluids by ongoing dehydration reactions (Fig. 12).

Geodynamic and thermo-mechanical models of ceased Farallon subduction include microplate capture, slab breakoff and the formation of a slab windows beneath the overriding North American plate (Nicholson et al. 1994; Wilson et al. 2005, e.g.). In settings where the ridge is near the trench (Fig. 12a), the buoyancy of the relatively young and hot, downgoing slab compensates for slab pull, spreading may slow and the coupling between the two spreading plates increases. As a result, when slab-pull forces exceed the strength of the subducting plate, the downgoing slab tears and becomes accommodated in the mantle, and the two originally

spreading plates become effectively one (McCrory et al. 2009). Such a breakoff scenario is considered for the ceased subduction and capture of Monterey microplate in central California. When the slab teared beneath the overriding North American plate, the previously subducting Monterey microplate became attached to the Pacific plate. Asthenosphere that filled the forming slab window supplied a shallow heat source in direct contact with the overlying crust (Fig. 12b).

Based on this geodynamic scenario, Kirby et al. (2002) combined a detailed thermal model with a kinetic reaction model of serpentinite formation and dehydration to illustrate that the temperature increase following the migration of the Mendocino Triple Junction could drive continued prograde dehydration of serpentinized mantle for tens of millions of years resulting in a large and sustained flux of water into the overlying crust. Numerical modelling and petrological constraints have been used to propose that less than 10 % of the mantle wedge were molten after the heat pulse following Mendocine triple junction passage (Schmitt et al. 2006). In turn, more than 90 % of the hydrated mantle wedge material would remain in place following MTJ passage and gradually dehydrate (Kirby et al. 2002).

Fulton and Saffer (2009) expanded this idea and demonstrated that dehydration of a persistent mantle wedge could account for the fluid overpressure (Fig. 6c) and the mantle-derived He signal observed near and within the SAFOD. Their calculations are based on dehydration of a volume of serpentinized mantle wedge corresponding to that of the modern mantle wedge beneath Cascadia sustained since the initiation of the SAF system, and on coupled heat and fluid flow modelling through a permeable upper crust with prescribed permeability. They further argue that fluid flux from a mantle wedge fluid source could generate isolated high

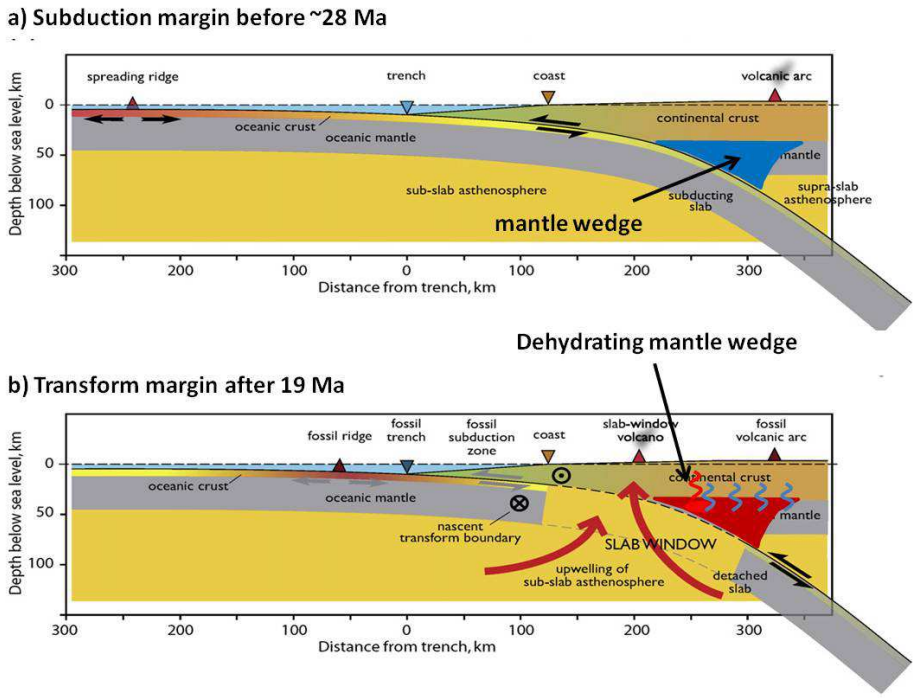

Fig. 12 Schematics of the evolution of the San Andreas transform margin, including capture of the remnant Monterey microplate, formation of a slab window and initiation of the transform margin near the slab tear, more than $\sim$ 19 Ma ago. A serpentinized mantle wedge may have formed during the subduction history, and dehydration of this wedge may be an ongoing process (Fulton and Saffer 2009). Figure modified after McCrory et al. (2009).

fluid pressure pockets within an impermeable fault zone that acts as a barrier for fluid flow.

These considerations suggest that the HCZ imaged with MT could correspond to the hypothesized dehydrating mantle wedge. The MT models are further consistent with the modelling scenario of Fulton and Saffer (2009) in suggesting permeable pathways through the crust into the creeping fault system. However, the geometrical interrelation between the resistivity model and the model of Fulton and Saffer are inconsistent. The MT model images the speculative fluid source

20-40 km west of the SAF. The MT models further suggest that crustal pathways near SAFOD have an oblique, westward dipping geometry, running from the eastern fault block in the upper crust across the mid-crustal SAF to lower crustal and upper mantle levels beneath and west of the SAF.

Fulton and Saffer (2009) placed the mantle wedge from the SAF eastward, based on the obervation that mantle-derived He signals are elevated within the eastern fault block. Kirby et al. (2002) suggested that the mantle wedge should be at a distance of $60 - 250$ km from the former trench, depending on variations in original slab dip. This distance range would agree with the model assumption of Fulton and Saffer (2009), placing the wedge east of the present SAF, as well as with the position of the HCZ west of the fault trace.

Fulton and Saffer (2009) assumed further that upper crustal fluid flow would be controlled by NE dipping faults and fractures within the country rock, with the ability to focus fluids into the brittle SAF. They argued that NE-dipping faults could be critically stressed and may thus act as the most permeable pathways for fluid flow (Townend and Zoback 2000). However, thrust faults in the Parkfield region penetrating into Franciscan rocks to mid-crustal levels or deeper, such as the Coalinga thrust and the San Joaquin thrust, exhibit a SW dipping geometry, whereas back-thrusts at the base of the Great Valley sequence, such as the Waltham Canyon thrust, exhibit dip to the NE (cf. Guzofski et al. 2007, Figure 5). Carena (2006) identified from earthquake data an active fault just east of the SAF near Parkfield that abuts the SAF near the bottom of the seismogenic crust (~ 15 km) (dashed line T in Fig. 7a). Furthermore, seismic waveform inversion across the SAF at SAFOD inferred a SW dipping reflector segment at lower crustal depth west of the SAF (element H in Fig. 7a, cf. Bleibinhaus et al.

2007), which could represent the lower crustal extension of the thrust described by Carena. Hence, there are strong indications for the existence of SW dipping faults, which could provide open pathways for fluid flow from a mantle wedge fluid source located west of the SAF (the HCZ), across the SAF and into the eastern fault block.

3.4 Relation with the slab window geometry

In the previous sections, we presented arguments that the HCZ may correspond to a ductile deformation zone and that fluids within the HCZ may be sourced in a dehydrating mantle wedge. If so, the position would provide constraints on the geometrical setting of the slab window model.

The slab window model implies that a proto-San Andreas was initiated near the slab tear zone, when the slab remnant was captured by the Pacific plate and induced transform motion into the overriding continental North-American block, facilitated by a thermal pulse of upwelling astenospheric material (Fig. 12). Geological evidence (e.g. Wilson et al. 2005), in agreement with thermo-mechanical and kinematic modelling (Nicholson et al. 1994), show that the main strand of the brittle fault system jumped inland in several discrete steps to its current position, the San Andreas fault. These jumps were associated with inland diffusion of the ductile roots of the deformation system, probably triggered by lower crustal and upper mantle temperature diffusion, or controlled by integrated lithospheric strength variations (Popov 2009). This means that the ductile roots of the fault system have been positioned between the ductile initiation zone of the SAF along the edge of the captured slab and its present position, possibly corresponding

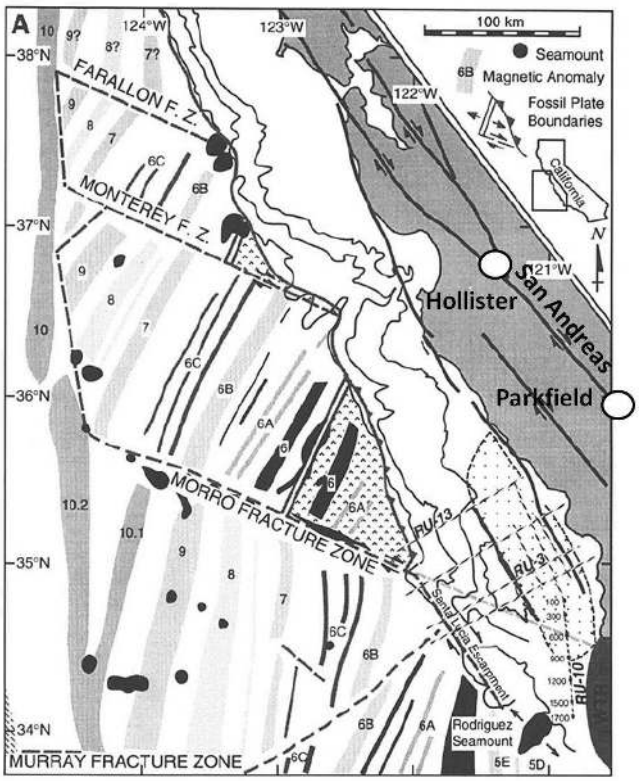

Fig. 13 Magnetic anomaly map showing the offshore extent of the remant Monterey microplate in Central California (Figure after Nicholson et al. 1994).

to teh source region of NVT near-vertically below the seismically defined crustal protion of the fault offset towards the coast to the west.

The position of slab tear with respect to the spreading center is debated. Wilson et al. (2005) located the Monterey slab tear near the present coastline based on seismic imaging of the fossil plate fragment beneath the continental margin (Tréhu 1991) and on the distribution of forearc volcanism. Theoretical studies that model slab tears typically assume a much deeper location for detachment , at depths of 50–100 km where dehydration embrittlement of the slab is thought to occur. McCrory et al. (2009) propose that the tear can occur at much shallower depths of

about 25 km, up-dip of a 450 °C thermal threshold that marks the brittle–ductile transition for quartzo-feldspathic-rich rocks in the accretionary prism. In either case, the ductile roots of the SAF system would be located inland of the breakoff-region. If the HCZ images the ductile deformation zone then this would place the slab tear necessarily to the west of the HCZ, in agreement with models of Wilson et al. (2005),McCrory et al. (2009) and Popov (2009).

The slab geometry sketched in Figure 12 implies that the mantle wedge would have developed further inland, i.e. east of the breakoff zone, and that this region can thus not coincide with the HCZ. However, it must be taken into account that the present-day geometry is integrating tectonic processes over geological time, including hundreds of kilometers of transform motion along the continental margin. This means, that the actual location of the HCZ region provides constraints on the result of tectonic processes, and not directly on its intial conditions.

Remnants of the Monterey microplate exist offshore central California. Magnetic anomaly maps of fossil spreading centers (Figure 13, after Nicholson et al. 1994) and documented phases of volcanism (Wilson et al. 2005) indicate that spreading and subduction of individual fragments of the Monterey Microplate ceased between 20 Ma and 16 Ma, from south to north. It is important to note that subduction of the segmented ridge system has been characterized by episodic ridge deaths interspersed with intervals of fracture zone subduction (McCrory et al. 2009) and is an ongoing process in the Cascades.

Therefore, slab tear and mantle wedge formation may have occurred at variable distance from the coast and at different times, and separately for individual slab fragments. Subsequent reorganization of the continental margin by transform motion along the evolving SAF may have further complicated geometrical

relationships, and could even have co-located slab window and mantle wedge at some points. Recently presented seismological mantle tomography (Schmandt and Humphreys 2010) images the actively subducting slab in the mantle beneath the Cascades as an elongated, trench-parallel high-velocity perturbation. In contrast, velocity structure beneath the Californian Coast Ranges is more heterogeneous in the upper mantle (model has been presented for >90 km depth), indicating that the slab window is not a continous structure along coastal California and that its evolution was variable along-strike.

Note finally that the inland extrapolation of the Farallon and Monterey Fracture Zones abut the SAF approximately at Hollister and Parkfield, respectively (Figure 13). The Monterey Fracture zones separates two fragments of the microplate, and the fossile spreading ridges are displaced along this fracture zone. As outlined before, it is unclear how far the Monterey microplate and thus the Fracture Zones extend beneath the continental margin, but it is imaginable that the geometry of the slab tear is dependent on the distance to the individual ridges and thus discontinues across the Fracture zone. This would add another complication to the geometrical setting beneath the continental edge.

4 Summary and Conclusions

Fluids are believed to play a key role in the mechanics and dynamics of faulting. MT is powerful in delineating high conductivity zones, and aqueous fluids residing in interconnected porosity networks often provide a plausible explanation. Therefore, MT can help to constrain fluid-related tectonic processes by illuminating the distribution of fluids and fluid pathways. However, to obtain a deeper un-

derstanding of the resistivity structure, results from other disciplines have to be incorporated.

In this paper, we combined the MT results from the San Andreas fault zone with other geophysical and geochemical observations, and geodynamic models to address the source of fluids and mechanisms that may have generated pathways. In doing so, a scenario evolved that fits into modern geodynamic models, and that can help to explain variations in the seismic behavior of the fault. However, many studies, including the existing regional scale MT studies, focused on the Parkfield-Cholame segment of the SAF in Central California, where the fault is transitional from mechanical lock to aseismic creep. Therefore, it is an open question whether or not fluid-based scenarios presented here are representative for larger portions of the fault.

Along the Parkfield-Cholame segment, regional scale MT profiles identified a lower crustal and upper mantle high-conductivity zone offset from the SAF trace towards the coast (Becken et al. 2011), which could image a dehydrating mantle wedge region (Kirby et al. 2002; Fulton and Saffer 2009). Fluids sourced in the mantle wedge find pathways into weak crustal zones here proposed to coincide spatially with exhumation paths of serpentinite (Kirby et al. 2002), and imaged as uniterrupted conductive zones (Becken et al. 2008). These pathways intersect the SAF at depth near the brittle ductile transition zone, and feed a fluid reservoir in the eastern fault block (Unsworth and Bedrosian 2004; Becken et al. 2008). This could explain SAFOD observations of fluid chemistry and hydrology (Zoback et al. 2006; Wiersberg and Erzinger 2007), including overpressured fluids in the eastern fault block (Johnson and McEvilly 1995; Zoback et al. 2010). Both, serpentinite or reaction products derived from serpentinite, such as talc (Moore and Rymer 2007),

and high-pressure fluids (Irwin and Barnes 1975; Rice 1992; Fulton and Saffer 2009) are therefore closely associated and could be responsible for the weakness of the fault where it exhibits aseismic creep.

However, SAFOD observations do not strictly support the idea that high-pressure fluids play an important role for fault creep, because *in situ* observations from the fault core, where it was drilled, provided no evidence for elevated fluid pressures. This suggests that either the point where the SAF was intersected by the SAFOD borehole is not representative for much of fault zone, or that fault zone models involving high fluid pressures must be reconciled.

Where the fault is locked, the crust is overly resistive between the inferred mantle wedge region and the SAF (Becken et al. 2011), and serpentinite occurrences are unknown. This suggests that serpenite was not exhumed along the locked segment and that fluids are trapped near the mantle wedge source region. Ongoing dehydration and fluid trapping in this region could result in high fluid pressures, and trigger brittle-like rock failure in nearby critically stressed domains. This agrees with the presence of near-lithostatic fluid pressures inferred for the source region of non-volcanic tremor near Cholame (Nadeau and Dolenc 2005; Thomas et al. 2009; Shelly 2010).

Existing MT studies at other locations than the Parkfield-Cholame area, such as Hollister or Carrizo Plain, are limited in their spatial extent and period range, and can not resolve lower crustal or upper mantle structure. If fluids of mantle origin play an important role for the creeping behavior of the fault, as inferred for the Parkfield region, then it can be expected that a deep fluid source as well as crustal fluid paths exist along the creeping portions of the SAF. In turn, fluids trapped below the (mid-)crust could be characteristic for the locked segment, as

inferred for the Cholame region. Expanded MT investigations at Hollister and Carrizo Plain, or at other locations along the SAF, could probe the deeper roots and test for systematic, fluid-related characteristics of the creeping and locked segments and complement the scenario developed for the Parkfield-Cholame area.

In the upper few kilometers of the fault, active deformation facilitates the formation of a fault zone conductor (FZC). A FZC has been observed at different positions along the creeping segment and its magnitude depends on fault activity. Repeated cycles of healing and shearing could be responsible for the formation of broad (several hundreds of meters) fault damage zones. In a detailed investigation, Ritter et al. (2005) exemplified how the geometry and conductivity of a FZC in combination with seismicity helps to decipher architectural units and hydraulic characteristics of the fault zone.

The models and mechanisms proposed from the MT data suggest occurrence and supply of fluids and the formation of fluid networks at all depth levels, from the upper crust into the upper mantle, with apparent important implications for the mechanical state of the SAF at a particular segment. Furthermore, MT results may help constrain geodynamic models of the continental margin of western North America.

Acknowledgements I wish to express my sincere thanks to the Program Committee and LOC of the Giza workshop, who offered me a chance to prepare and deliver this review. We also thank the guest editors of the review volume, T. Korja and N. Palshin for their guidance and patience.

References

L. Aranovich, N. Bortnikov, S. Bushmin, O. Vikent` eva, E. Dubinina, V. Kozlovskii, and Yu. Lebedeva. Fluid flows in regional deformation zones. *Petrology*, 17:389–409, 2009. ISSN 0869-5911.

M. Becken and H. Burkhardt. An ellipticity criterion in magnetotelluric tensor analysis. *Geophys. J. Int.*, 159:69–82, 2004.

M. Becken, O. Ritter, S. K. Park, P. A. Bedrosian, U. Weckmann, and M. Weber. A deep crustal fluid channel into the San Andreas fault system near Parkfield, California. *Geophys. J. Int.*, 173:718–732, 2008.

M. Becken, O. Ritter, P. A. Bedrosian, and U. Weckmann. Deep electrical conductivity in the non-volcanic tremor region at the San Andreas fault. *submitted*, ??:??, 2011.

P. A. Bedrosian, M. J. Unsworth, G. D. Egbert, and C. H. Thurber. Geophysical images of the creeping segment of the San Andreas fault: implications for the role of crustal fluids in the earthquake process. *Tectonophysics*, 385:137–156, 2004.

N. Bennington, C. Thurber, and S. Roecker. Threedimensional seismic attenuation structure around the SAFOD site, Parkfield, California. *Bull. Seismol. Soc. Am.*, 98:2934–2947, 2008.

F. Bleibinhaus, J. A. Hole, T. Ryberg, and G. S. Fuis. Structure of the California Coast Ranges and San Andreas Fault at SAFOD from seismic waveform inversion and reflection imaging. *J. geophys. Res.*, 112:B06315, 2007.

Roland Bürgmann and Georg Dresen. Rheology of the Lower Crust and Upper Mantle: Evidence from Rock Rechanics, Geodesy, and Field Observations . *Annu. Rev. Earth Planet. Sci.*, 36:531–567, 2008.

S. Buske, S. Gutjahr, S. Rentsch, and S. A. Shapiro. Application of Fresnel-Volume-Migration to the SAFOD2003 data set. In *EAGE 69th annual meeting and technical exhibition, Extended Abstracts*, 2007.

J. Byerlee. Friction, overpressure and fault normal compression. *Geophys. Res. Lett.*, 17: 2109–2112, 1990.

J. S. Caine, J. P. Evans, C. P. Evans, and C. P. Foerster. Fault zone architecture and permeability structure. *Geology*, 24:1125–1128, 1996.

S. Carena. 3-D Geometry of Active Deformation East of the San Andreas Fault Near Parkfield, California. *AGU Fall Meeting Abstracts*, pages C178+, December 2006.

J. Chéry, M. D. Zoback, and S. Hickman. A mechanical model of the San Andreas fault and SAFOD pilot hole stress measurements. *Geophys. Res. Lett.*, 31:L15S13, 2004.

J. A. D. Connolly and Y. Y. Podladchikov. Fluid flow in compressive tectonic settings: Implications for midcrustal seismic reflectors and downward fluid migration. *J. geophys. Res.*, 109:B04201, 2004.

S. F. Cox. Coupling between deformation, fluid pressures, and fluid flow in ore-producing hydrothermal systems at depth in the crust. In J. W. Hedenquist, J. F. H. Thompson, R. J. Goldfarb, and J. P. Richards, editors, *Economic Geology 100th Anniversary Volume*, Econ. Geol., pages 39–76. 2005.

William R. Dickinson, Lewis I. Rosenberg, H. Gary Greene, Stephan A. Graham, Joseph C. Clark, Gerald E. Weber, Steven Kidder, W. Gary Ernst, and Earl E. Brabb. Net dextral slip, Neogene San Gregorio, Hosgri fault zone, coastal California: Geologic evidence and tectonic implications. *Geological Society of America Special paper 391*, pages 1–43, 2005.

D. Eberhart-Philips, W. D. Stanley, B. D. Rodriguez, and W. J. Lutter. Surface seismic and electrical methods to detect fluids related to faulting. *J. geophys. Res.*, 100(B7):12919–12936, 1995.

P. M. Fulton and D. M. Saffer. Potential role of mantle-derived fluids in weakening the San Andreas Fault. *J. geophys. Res.*, 114:B07408, 2009.

Y. Gueguen and V. Palciauskas. *Introduction to the physics of rocks*. Princeton University Press, Princeton, NJ, 1994.

Aysan Gürer and Murat Bayrak. Relation between electrical resistivity and earthquake generation in the crust of West Anatolia, Turkey. *Tectonophysics*, 445:49–65, 2007.

C. A. Guzofski, J. H. Shaw, G. Lin, and P. M. Shearer. Seismically active wedge structure beneath the Coalinga anticline, San Joaquin basin, California. *J. geophys. Res.*, 112: B03S05, 2007.

Z. Hashin and S. Shtrikman. Electrical conductances of aqueous sodium chloride solutions from 0 to 800Â° and at pressures to 4000 bars. *J. Appl. Phys.*, 33:3125–3131, 1962.

S. Hickman, M. Zoback, and W. Ellsworth. Introduction to special section: Preparing for the San Andreas Fault Observatory at Depth. *Geophys. Res. Lett.*, 31:L12S01, 2004.

A. Hoffmann-Rothe, O. Ritter, and C. Janssen. Correlation of electrical conductivity and structural damage at a major strike-slip fault in northern Chiley. *J. geophys. Res.*, 109: B10101, 2004.

J. A. Hole, T. Ryberg, A. K. Sharma, and S. G. Fuis. Seismic velocity structure from a refraction - reflection survey across the San Andreas Fault at SAFOD. San Francisco, 2004. AGU Fall meeting.

W. P. Irwin. *Geology and plate-tectonic development*, chapter 3. The San Andreas fault system in California: United States Geological Survey, Professional Paper 1515, 1990.

W. P. Irwin and I. Barnes. Effect of geologic structure and metamorphic fluids on seismic behavior of the San Andreas fault system in central and northern california. *Geology*, 3: 713–716, 1975.

G. R. Jiracek, V. M. Gonzalez, T. G. Caldwell, P. E. Wannamaker, and D. Kilb. Seismogenic, electrically conductive, and fluid zones at continental plate boundaries in New Zealand, Himalaya, and California-USA. In D. Okaya, T. Stern, and F. Davey, editors, *Geotectonic Investigation of a Modern Continent-Continent Collisional Orogen: Southern Alps, NZ*, volume 175, pages 347–369. Geophysical Monograph Series AGU, 2007.

P. A. Johnson and T. V. McEvilly. Parkfield seismicity: Fluid-driven. *J. geophys. Res.*, 100: 12937–12950, 1995.

K. N. Kappler, H. F. Morrison, and G. D. Egbert. Long-term monitoring of ULF electromagnetic fields at Parkfield, California. *J. geophys. Res.*, 115:B04406, 2010.

B. M. Kennedy, Y. K. Kharake, W. C. Evans, A. Ellwood, D. J. DePaolo, J. Thordsen, and R. H. Mariner. Mantle Fluids in the San Andreas Fault System, California. *Science*, 278: 1278–1281, 1997.

Y. K. Kharaka, J. J. Thordsen, W.C. Evans, and B.M. Kennedy. Geochemistry and hydromechanical interactions of fluids associated with the San Andreas fault system, California. In W.C. Haneberg, P.S. Mosely, J.C. Moore, and L.B. (Eds.) Goodwin, editors, *Faults and Subsurface Fluid Flow in the Shallow Crust.*, volume 113 of *Geophysical Monograph*, pages 129–148. American Geophysical Union, Washington, 1999.

S. H. Kirby, K. Wang, and T. Brocher. A possible deep, long-term source for water in the Northern San Andreas Fault system: A ghost of Cascadia subduction past? *Eos Trans. AGU*, 83:Fall Meet. Suppl., Abstract S22B–1038, 2002.

Y. D. Li and P. E. Malin. San Andreas Fault damage at SAFOD viewed with fault-guided waves. *Geophys. Res. Lett.*, 35:L08304, 2008.

R.L. Mackie, D. W. Livelybrooks, T. R. Madden, and J. C. Larsen. A magnetotelluric investigation of the San Andreas Fault at Carrizo Plain, California. *Geophys. Res. Lett.*, 24: 1847–1850, 1997.

T. R. Madden, G. A. LaTorraca, and S. K. Park. Electrical conductivity variations around Palmdale section of the San Andreas Fault zone. *J. geophys. Res.*, 98:795–808, 1993.

Patricia A. McCrory, Douglas S. Wilson, and Richard G. Stanley. Continuing evolution of the Pacific-Juan de Fuca-North America slab window system - A trench-ridge-transform example from the Pacific Rim. *Tectonophysics*, 464:30–42, 2009.

D. K. McPhee, R. C. Jachens, and C. M. Wentworth. Crustal structure across the San Andreas Fault at the SAFOD site from potential field and geologic studies. *Geophys. Res. Lett.*, 31:L12S03, 2004.

Diane E. Moore and Michael J. Rymer. Talc-bearing serpentinite and the creeping section of the San Andreas fault. *Nature*, 448:795–797, 2007.

R. M. Nadeau and D. Dolenc. Nonvolcanic Tremors Deep Beneath the San Andreas Fault. *Science*, 21:389, 2005.

C. Nicholson, C. C. Sorlien, T. Atwater, J. C. Crowell, and B. P. Luyendyk. Microplate Capture, rotation of the western Transverse Ranges, and initiation of the San Andreas transform as a low-angle fault system. *Geology*, 22:491–495, 1994.

K. Obara. Nonvolcanic Deep Tremor Associated with Subduction in Southwest Japan. *Science*, 31:1679–1681, 2002.

A. A. Ozacar and G. Zandt. Crustal structure and seismic anisotropy near the San Andreas Fault at Parkfield, California. *Geophys. J. Int.*, 178:1098–1104, 2010.

Benjamin M. Page, George A. Thompson, and Robert G. Coleman. Late Cenozoic tectonics of the central and southern Coast Ranges of California. *GSA Bulletin*, 110:846–876, 1998.

S. K. Park, J. C. Larsen, and T.-C. Lee. Electrical resistivity changes not observed with the 28 September 2004 M6.0 Parkfield earthquake on the San Andreas fault, California. *J. geophys. Res.*, 112:B12305, 2007.

E. Pili, B. M. Kennedy, M. S. Conrad, and J. P. Gratier. Isotope constraints on the involvement of fluids in the San Andreas fault. *EOS, Trans. AGU*, 79:229–230, 1998.

A. A. Popov. *Three-dimensional thermo-mechanical modeling of deformation at plate boundaries: case study San Andreas Fault System.* PhD thesis, Potsdam University, 2009.

A. S. Quist and A. L. Marshall. Electrical conductances of aquaeous sodium chloride solutions from 0 to 800° and at pressures to 4000 bars. *Journal of Physical Chemistry*, 72:684–703, 1968.

J. R. Rice. Fault stress states, pore pressure distributions, and the weakness of the san andreas fault. In B. Evans and T.-F Wong, editors, *Fault Mechanics and Transport Properties of Rocks*, pages 475–503. Academic, San Diego, Calif., 1992.

O. Ritter, U. Weckmann, T. Vietor, and V. Haak. A Magnetotelluric study of the Damara Belt in Namibia 1. Regional scale conductivity anomalies. *Phys. Earth Planet. Inter.*, 138: 71–90, 2003.

O. Ritter, A. Hoffmann-Rothe, P. A. Bedrosian, U. Weckmann, and V. Haak. Electrical conductivity images of active and fossil fault zones. In *in High-Strain Zones: Structure and Physical Properties, Bruhn, D. and Burlini, L. (eds.)*, volume 245, pages 165–186. Geological Society of London Special Publications, 2005.

T. Ryberg, G. S. Fuis, K. Bauer, J. A. Hole, and F. Bleibinhaus. Upper-Crustal Reflectivity of the Central California Coast Range Near the San Andreas Fault Observatory at Depth (SAFOD), USA. *AGU Fall Meeting Abstracts*, pages A441+, December 2005.

T. Ryberg, C. Haberland, G. S. Fuis, W. L. Ellsworth, and D. R. Shelly. Locating non-volcanic tremor along the San Andreas Fault using a multiple array source imaging technique. *Geophys. J. Int.*, pages 1485–1500, 2010.

J. H. Sass, C. F. Williams, A. H. Lachenbruch, S. P. Galanis Jr, and F. V. Grubb. Thermal regime of the San Andreas fault near Parkfield, California. *J. geophys. Res.*, 102:27575–27585, 1997.

F. R. Schilling, G. M. Partzsch, H. Brasse, and G. Schwarz. Partial melting below the magmatic arc in the central andes deduced from geoelectromagnetic field experiments and laboratory data. *Phys. Earth Planet. Inter.*, 103:17–32, 1997.

Brandon Schmandt and Eugene Humphreys. Complex subduction and small-scale convection revealed by body-wave tomography of the western united states upper mantle. *Earth and Planetary Science Letters*, 297:435 – 445, 2010. doi: DOI: 10.1016/j.epsl.2010.06.047.

A. K. Schmitt, R. Romer, and J. Stimac. Geochemistry of volcanic rocks from the Geysers geothermal reservoir, Californian Coast Ranges. *Lithos*, 87:80–103, 2006.

U. Schmucker. *Anomalies of Geomagnetic Variations in the Southwestern United States*. Univ. of California Press, Berkeley, 1970.

C. H. Scholz. *The Mechanics of Earthquakes and Faulting*. Cambridge University Press, 2nd edition, 2002.

S. Y. Schwartz and J. M. Rokosky. Slow slip events and seismic tremor at circum-pacific subduction zones. *Rev. Geophys.*, 45:RG3004, 2007.

D. R. Shelly. Migrating tremors illuminate deformation beneath the seismogenic San Andreas fault. *Nature*, 463:648–652, 2010.

D. R. Shelly, G. C. Beroza, S. Ide, and S. Nakamula. Low-frequency earthquakes in Shikoku, Japan and their relationship to episodic tremor and slip. *Nature*, 442, 2006.

D. R. Shelly, W. L. Ellsworth, T. Ryberg, C. Haberland, G. S. Fuis, J. Murphy, R. M. Nadeau, and R. Bürgmann. Precise location of San Andreas Fault tremors near Cholame, California using seismometer clusters: Slip on the deep extension of the fault? *Geophys. Res. Lett.*, 36:L01303, 2009.

A. M. Thomas, R. M. Nadeau, and R. Bürgmann. Tremor-tide correlations and near-lithostatic pore pressure on the deep San Andreas fault. *Nature*, 462:1048–1051, 2009.

C. Thurber, S. Roecker, H. Zhang, S. Baher, and W. Ellsworth. Fine-scale structure of the San Andreas fault zone and location of the SAFOD target earthquakes. *Geophys. Res. Lett.*, 31:L12S02, 2004.

J. Townend and M. D. Zoback. How faulting keeps the crust strong. *Geology*, 28:399–402, 2000.

J. Townend and M. D. Zoback. Regional tectonic stress near the San Andreas Fault in central and southern California. *Geophys. Res. Lett.*, 31:L15S11, 2004.

A. M. Tréhu. Tracing the subducted oceanic crust beneath the central California continental margin: results from ocean bottom seismometers deployed during the 1986 PG&E/EDGE experiment. *J. geophys. Res.*, 96:6493–6506, 1991.

M. J. Unsworth. Magnetotelluric Studies of Active Continent-Continent Collisions. *Surv. Geophys.*, 31:137–161, 2010.

M. J. Unsworth and P. Bedrosian. Electrical Resistivity structure at the SAFOD site from magnetotelluiric exploration. *Geophys. Res. Lett.*, 31:L12S05, 2004.

M. J. Unsworth, P. E. Malin, G. D. Egbert, and J. R. Booker. Internal structure of the San Andreas fault at Parkfield, California. *Geology*, 25:359–362, 1997.

M. J. Unsworth, G. D. Egbert, and J. R. Booker. High resolution electromagnetic imaging of the San Andreas Fault in Central California. *J. geophys. Res.*, 104:1131–1150, 1999.

M. J. Unsworth, P. Bedrosian, M. Eisel, G. D. Egbert, and W. Siripunvaraporn. Along strike variations in the electrical structure of the San Andreas Fault at Parkfield, California. *Geophys. Res. Lett.*, 27:3021–3024, 2000.

P. E. Wannamaker, T. Grant Caldwell, George R. Jiracek, Virginie Maris, Graham J. Hill, Yasuo Ogawa, Hugh M. Bibby, Stewart L. Bennie, and Wiebke Heise. Fluid and deformation regime of an advancing subduction system at Marlborough, New Zealand. *Nature*, 460: 733–736, 2010.

T. Wiersberg and J. Erzinger. A helium isotope cross-section study through the San Andreas Fault at seismogenic depths. *Geochemistry Geophysics Geosystems*, 8:Q01002, 2007.

H. Wiese. Geomagnetische Tiefentellurik Teil ii: Die Streichrichtung der Untergrundstrukturen des elektrischen Widerstandes, erschlossen aus geomagnetischen Variationen. *Geofis. Pura e Appl.*, 52:83–103, 1962.

D. S. Wilson, Patricia A. McCrory, and Richard G. Stanley. Implications of volcanism in coastal California for the Neogene deformation history of western North America. *Tectonics*, 24: TC3008, 2005.

H. Zhang, C. Thurber, and P. Bedrosian. Joint inversion for vp, vs, and vp/vs at safod, parkfield, california. *Geochem. Geophys. Geosyst*, 10:Q11002, 2009.

M. Zoback, J. Townend, and B. Grollimund. Steady-State Failure Equilibrium and Deformation of Intraplate Lithosphere. *International Geology Review*, 44:383–401, 2002.

M. Zoback, S. Hickman, and W. Ellsworth. Structure and properties of the San Andreas fault in central California: Preliminary results from the SAFOD experiment. In *Geophys. Res. Abstracts*, volume 8. EGU, 2006.

M. Zoback, S. Hickman, and W. Ellsworth. Scientific drilling into the San Andreas fault zone. *Eos Trans. AGU*, 91:197–199, 2010.